arXiv:2008.08342v2 [cond-mat.dis-nn] 24 Nov 2020

Structure Learning in Inverse Ising Problems Using ℓ_2-Regularized Linear Estimator

Xiangming Meng[‡*] Tomoyuki Obuchi[†] Yoshiyuki Kabashima[* ‡]

February 15, 2022

Abstract

The inference performance of the pseudolikelihood method is discussed in the framework of the inverse Ising problem when the ℓ_2-regularized (ridge) linear regression is adopted. This setup is introduced for theoretically investigating the situation where the data generation model is different from the inference one, namely the model mismatch situation. In the teacher-student scenario under the assumption that the teacher couplings are sparse, the analysis is conducted using the replica and cavity methods, with a special focus on whether the presence/absence of teacher couplings is correctly inferred or not. The result indicates that despite the model mismatch, one can perfectly identify the network structure using naive linear regression without regularization when the number of spins N is smaller than the dataset size M, in the thermodynamic limit $N \to \infty$. Further, to access the underdetermined region $M < N$, we examine the effect of the ℓ_2 regularization, and find that biases appear in all the coupling estimates, preventing the perfect identification of the network structure. We, however, find that the biases are shown to decay exponentially fast as the distance from the center spin chosen in the pseudolikelihood method grows. Based on this finding, we propose a two-stage estimator: In the first stage, the ridge regression is used and the estimates are pruned by a relatively small threshold; in the second stage the naive linear regression is conducted only on the remaining couplings, and the resultant estimates are again pruned by another relatively large threshold. This estimator with the appropriate regularization coefficient and thresholds is shown to achieve the perfect identification of the network structure even in $0 < M/N < 1$. Results of extensive numerical experiments support these findings.

1 Introduction

The advent of massive data across various scientific disciplines has led to widespread use of the classical Ising model as a tool for data modeling [1]. Recent applications that have spurred this trend include retinal neutrons, reconstruction of neural and gene regulatory networks, and

[*]Institute for Physics of Intelligence and Department of Physics, Graduate School of Science, The University of Tokyo, 7-3-1, Hongo, Tokyo 113-0033, Japan

[†]Department of Systems Science, Graduate School of Informatics, Kyoto University, Yoshida Hon-machi, Sakyo-ku, Kyoto-shi, Kyoto 606-8501, Japan

[‡]Corresponding author. E-mail: meng@g.ecc.u-tokyo.ac.jp

determination of the three-dimensional structure of proteins in biological sciences [1, 2, 3, 4, 5, 6]. Inference based on the Ising model is called the inverse Ising problem or Boltzmann machine learning, which refers to reconstructing the parameters and structure of an Ising model on the basis of samples of spin configurations. The maximum likelihood (ML) method is one of the main methods for solving this problem. However, in general, ML is computationally intractable for a large system. Two popular approaches have been developed to address this problem. The first is to approximate the ML using approximations such as Monte Carlo sampling [7, 8, 9] and mean-field approximations [10, 11, 12]. The second approach introduces some local cost function that is easier to optimize instead of directly maximizing the likelihood function. One of the most effective examples of the latter is the pseudolikelihood (PL) method [2, 13, 14, 15], which approximates the likelihood function as the product of conditional likelihood functions. A prominent advantage of the PL method is that one can independently estimate the couplings associated with each spin, as the local couplings directly connected to a single spin are isolated from the others, thus simplifying the implementation.

Recently, some theoretical analyses revealing the inference accuracy of the PL method have been conducted using methods of statistical mechanics [3, 4, 5, 6]. For example, in [5], assuming that data are drawn independently from an equilibrium Ising model, the learning performance of the PL method with a local cost function was studied for fully connected Ising models using a combination of the replica method and the cavity method [16, 17, 18]. Subsequently, in [6], some of the present authors extended the analysis to sparse couplings. The inverse Ising problem with sparse couplings has a practical relevance in structure learning of graphical models and a number of early studies are found [2, 14, 19, 20, 21, 22, 23, 24, 25]. These analyses provide a firm theoretical basis for inverse Ising problems.

In the above studies, the postulated model used in the inference stage covers the true model that generates the data. However, such an assumption does not necessarily hold in practical situations, because the data-generating model is generally unknown *a priori*. Therefore, it is important to evaluate the learning performance of the popular PL method in model mismatch cases, which is the main focus of this study.

Specifically, within the teacher-student scenario, we examine the inference performance of the PL method when ℓ_2-regularized (ridge) linear regression is applied to data generated from the teacher Ising model with sparse couplings. The ridge regression is very simple but widely used in practical situations of data analysis, and thus is appropriate as a starting point for the present purpose. Our main question is whether the presence/absence of teacher coupling can be correctly inferred or not even in this mismatched case. To answer this question, we employ similar analytical techniques to those in [6]: we use the replica and cavity methods and take the thermodynamic limit where the number of spins N goes to infinity and the dataset size M is proportional to N as $M = \alpha N$ with $\alpha = \mathcal{O}(1)$; furthermore we assume the tree-like structure of the network of the teacher couplings and generalize the ansatz in [6] about the mean estimates of couplings on an assumed support. This generalized ansatz enables us to systematically treat the effect of the regularization.

As a result, we find that the ℓ_2 regularization causes undesirable biases in the overall coupling

estimates while without regularization no such biases exist for the estimates on the set of absent teacher couplings. This indicates that for $\alpha = M/N > 1$ the perfect recovery of the network structure is possible by the naive linear regression without regularization, since the fluctuation of the estimates vanishes in the thermodynamic limit as in the matched case [6] and thus we can effectively prune false positive couplings by a reasonable threshold. Meanwhile in the case of $\alpha \leq 1$, the regularization is necessary for obtaining the estimates and thus the biases are unavoidable, which makes the perfect recovery difficult. To overcome this, we further quantitatively analyze those biases, and find that they decay exponentially fast as the distance from the center spin chosen in the PL method grows. This finding motivates us to introduce a two-stage estimator for systematically achieving the perfect recovery even for $\alpha \leq 1$. The actual procedures of this two-stage estimator are as follows. In the first stage, we perform the ridge regression and then prune the estimates with a certain threshold to obtain $\mathcal{O}(1)$ coupling estimates[1]. In the second stage, the naive linear regression without regularization is performed only on the remaining couplings at the end of the first stage: the number of remaining couplings is expected to be $\mathcal{O}(1)$ and thus the dataset size is effectively very large ($\alpha \gg 1$) and hence we can again eliminate false positive couplings by a reasonable threshold. These results thus finally provide a positive answer to our question: the perfect recovery is possible as long as $\alpha > 0$ even in the mismatched case! To support these analytical results, we also conduct numerical experiments on the random regular (RR) graph and the Erdős–Rényi (ER) graph. The result is fairly consistent with all the analytical predictions and thus supports our findings.

The remainder of this paper is organized as follows. Section 2 reviews the inverse Ising problem and some typical estimators. In addition, it presents the problem setup in the teacher-student scenario. Section 3 describes the statistical mechanics analysis of the ℓ_2-regularized linear estimator, drawing on previous studies [5, 6] for sparse couplings. Numerical simulations are conducted to evaluate the accuracy of the theoretical analysis, and Section 5 compares the experimental results with the theoretical analysis. Finally, Section 6 concludes the paper.

2 Inverse Ising Problem

Let us consider an Ising model with N binary spin variables $\boldsymbol{s} = (s_i = \pm 1)_{i=0}^{N-1}$, which follows the Boltzmann distribution

$$P_{\text{Ising}}(\boldsymbol{s}|\boldsymbol{J}, \boldsymbol{H}) = \frac{1}{Z_{\text{Ising}}} e^{\sum_{i<j} J_{ij} s_i s_j + \sum_i H_i s_i}, \tag{1}$$

where Z_{Ising} is the partition function and $\boldsymbol{J} = (J_{ij})_{ij} \in \mathbb{R}^{N \times N}$ and $\boldsymbol{H} = (H_i)_{i=0}^{N-1} \in \mathbb{R}^N$ are the couplings and external fields, respectively. In (1), the temperature is absorbed in $\boldsymbol{J}$ and $\boldsymbol{H}$. The standard goal of the inverse Ising problem is to learn the couplings $\boldsymbol{J}$ and external fields

[1] To facilitate perfect recovery, this threshold should be sufficiently small to ensure full recall. If this threshold is independent of the system size N, then the number of false positive couplings is expected to be $\mathcal{O}(1)$ if N is large enough, because the majority of the spins is far from the center spin in the PL method if we assume the tree-like network and thus the corresponding biases are negligibly small compared to the threshold.

$\boldsymbol{H}$ from a set of observations of spin snapshots $\mathcal{D}^M = \left\{\boldsymbol{s}^{(\mu)}\right\}_{\mu=1}^{M}$, where M denotes the number of samples in the dataset, i.e., dataset size. Especially, a particular interest is on learning the network structure composed of the couplings. Our main focus in this paper is to reveal whether the structure learning is possible or not based on the linear estimator with the ℓ_2 regularization, as detailed below.

2.1 Some Estimators

Here we summarize some estimators for the inverse Ising problem and also describe the motivations for evaluation of the linear estimator.

2.1.1 Maximum Likelihood Estimator

The canonical estimator in statistics is the one based on the maximum likelihood (ML) method and is defined as

$$\left\{\hat{\boldsymbol{J}}^{ML}, \hat{\boldsymbol{H}}^{ML}\right\} = \underset{\boldsymbol{J},\boldsymbol{H}}{\arg\min} \left\{ -\sum_{\mu=1}^{M} \log P_{\text{Ising}}\left(\boldsymbol{s}^{(\mu)} | \boldsymbol{J}, \boldsymbol{H}\right) \right\}. \tag{2}$$

This shows some useful properties such as consistency and asymptotic efficiency. However in the inverse Ising problem, the ML method suffers from the high computational complexity because the exponentially large computational cost with respect to (w.r.t.) N is needed to compute Z_{Ising}. Due to this limitation, other estimators than the ML one are usually practically chosen.

2.1.2 Maximum Pseudolikelihood Estimator

An alternative to the ML method is the pseudolikelihood (PL) method [13], which replaces the original likelihood with the conditional distribution $P\left(s_i | \boldsymbol{s}_{\setminus i}, \boldsymbol{J}_i, H_i\right)$ for each spin s_i, where $\boldsymbol{J}_i = \left(J_{ij}\right)_{j(\neq i)}$ is the coupling vector connected to spin s_i and $\boldsymbol{s}_{\setminus i}$ is the spin vector $\boldsymbol{s}$ excluding s_i. Specifically, for each i, the conditional distribution $P\left(s_i | \boldsymbol{s}_{\setminus i}, \boldsymbol{J}_i, H_i\right)$ is of the form

$$P\left(s_i | \boldsymbol{s}_{\setminus i}, \boldsymbol{J}_i, H_i\right) = \frac{1}{Z_i} e^{s_i\left(\sum_{j(\neq i)} J_{ij} s_j + H_i\right)}, \tag{3}$$

where $Z_i = 2\cosh\left(\sum_{j(\neq i)} J_{ij} s_j + H_i\right)$ is the site partition function. Consequently, the PL estimator is applied to each i separately, leading to

$$\left\{\hat{\boldsymbol{J}}_i^{PL}, \hat{H}_i^{PL}\right\} = \underset{\boldsymbol{J}_i, H_i}{\arg\min} \left\{ \sum_{\mu=1}^{M} \left(-s_i^{(\mu)} h_i\left(\boldsymbol{s}_{\setminus i}^{(\mu)}, \boldsymbol{J}_i, H_i\right) + \log 2\cosh(h_i\left(\boldsymbol{s}_{\setminus i}^{(\mu)}, \boldsymbol{J}_i, H_i\right)) \right) \right\}, \tag{4}$$

where $h_i\left(\boldsymbol{s}_{\setminus i}^{(\mu)}, \boldsymbol{J}_i, H_i\right) = \sum_{j(\neq i)} J_{ij} s_j + H_i$.

The PL method has two remarkable properties: consistency and locality [26]. Consistency means that the PL estimator converges to the true value when the dataset size M is sufficiently large. Locality means that each coupling vector $\boldsymbol{J}_i$ can be estimated independently, which leads

to low computational complexity. For obtaining the coupling estimates for all couplings, the PL estimator should be computed for all $i = 1, \cdots, N$ separately.

According to earlier studies [6, 19, 20, 21], the perfect recovery of the network structure is possible by this PL estimator. Its information theoretic limit when employed with the ℓ_1 regularization is derived in [21], showing that the perfect recovery is possible in the large N limit satisfying $M > k \log N$ with an appropriate constant $k > 0$. Meanwhile, when the regularization is absent, the perfect recovery is again shown to be possible in the large N limit satisfying $\alpha = M/N > 2$ in [6]. In the latter study, the direct values of the variance and bias of the estimator are computed by using the statistical mechanical methods, and we employ the same approach for analyzing the performance of the linear estimator in this study.

2.1.3 Linear Estimator

The simplest estimator in regression is linear one. Thus we propose a linear estimator for the inverse Ising problem as follows:

$$\{\hat{\boldsymbol{J}}_i, \hat{H}_i\} = \underset{\boldsymbol{J}_i, H_i}{\arg\min} \left\{ \sum_{\mu=1}^{M} \left(s_i^{(\mu)} - \sum_{j(\neq i)} J_{ij} s_j^{(\mu)} - H_i \right)^2 + \lambda N \sum_{j(\neq i)} J_{ij}^2 \right\}. \tag{5}$$

As for the PL method, we focus on a single spin and perform the learning locally also in this case. The ℓ_2 regularization is introduced to make the estimator well defined even in the underdetermined situation $\alpha < 1$ and the factor N is introduced for the scaling to be appropriate.

This estimator implies that the corresponding inference model is outside the parameter family of the generative model, and hence the model mismatch occurs. Consequently, this estimator does not show consistency. It thus becomes more nontrivial whether the perfect recovery of the network structure is possible or not. Since the linear estimator is largely superior to the ML and PL ones in terms of the computational complexity/analytical amenability, its advantage will be huge if the perfect recovery is shown to be possible even by this linear estimator. Below we tackle this problem, to eventually find a positive answer.

2.2 Problem Setup: Linear Estimator in Teacher-Student Scenario

In this paper, we investigate the properties of the above linear estimator in the teacher-student scenario. The dataset $\mathcal{D}^M = \left\{ \boldsymbol{s}^{(\mu)} \right\}_{\mu=1}^{M}$ is assumed to be generated independently from a teacher Ising model with couplings $\boldsymbol{J}^*$ and external fields $\boldsymbol{H}^*$. We denote by $[\cdot]_{\mathcal{D}^M}$ the expectation over the dataset $\mathcal{D}^M$ generated in this way, i.e.,

$$[\cdot]_{\mathcal{D}^M} = \sum_{\boldsymbol{s}^{(1)}, \ldots, \boldsymbol{s}^{(M)}} (\cdot) \prod_{\mu=1}^{M} P_{\text{Ising}} \left(\boldsymbol{s}^{(\mu)} | \boldsymbol{J}^*, \boldsymbol{H}^* \right). \tag{6}$$

For simplicity of analysis, the external fields are assumed to be zero in the following, i.e., $\boldsymbol{H}^* = 0$. Furthermore, we assume the teacher couplings' network is tree-like as in [6]. Representative

examples of such networks are the RR graph and the ER graph with small edge probability. Our main focus is on whether we can recover this network structure based on the linear estimator, or not.

Correspondingly, we mainly analyze the following three quantities related to the structure learning: the residual sum of square (RSS)

$$\mathcal{E} = \left\| \boldsymbol{J}_i^* - \hat{\boldsymbol{J}}_i \right\|_2^2, \tag{7}$$

the variance of the estimator, and the rates of correctly inferring the presence/absence of couplings. For judging the presence/absence of couplings, a judging scheme is needed and we implement this by thresholding the estimator: we introduce a certain threshold $K_{\rm th}$ and if $|\hat{J}_i| > K_{\rm th}$ then we judge the corresponding coupling is present, otherwise it is supposed to be absent. The true positive rate, the rate of correctly inferred to be present among the present couplings, is denoted as TP. Similarly, the true negative, false positive, and false negative rates are denoted by TN, FP, and FN respectively. *Precision* and *Recall*, common statistical measures of inference accuracy, are defined by these quantities as

$$\text{Precision} = \frac{TP}{TP+FP}, \ \text{Recall} = \frac{TP}{TP+FN}, \tag{8}$$

and we quantify the network recovery accuracy by these two quantities. The reason why we do not directly use TP and FP is the imbalance in the presence rate of couplings since we assume the sparse network.

Below we state how these quantities are computed by the statistical mechanical analysis.

3 Statistical Mechanical Analysis

In this section, we present the statistical mechanical analysis of the inference performance of the ℓ_2-regularized linear estimator (5) following the previous studies [5, 6]. In the following, we first present the statistical mechanical formulation of the problem, illustrating its basic idea and difficulty. Afterwards, details of how to tackle such difficulty are illustrated in Sections 3.1-3.4.

For simplicity and without loss of generality, we denote the index of the focused spin as 0 and the coupling vector to be inferred by $\boldsymbol{J}$, where the index 0 is omitted. Following the standard prescription of statistical mechanics, the Hamiltonian corresponding to the cost function (5) is

$$\begin{aligned}
\mathcal{H}\left(\boldsymbol{J}|\mathcal{D}^M\right) &= \sum_{\mu=1}^{M}\left(s_0^{(\mu)} - \sum_{j=1}^{N-1} J_j s_j^{(\mu)}\right)^2 + \lambda N \sum_{j=1}^{N-1} J_j^2 \\
&= \sum_{\mu=1}^{M} \Phi\left(s_0^{(\mu)} h^{(\mu)}\right) + \lambda N \sum_{j=1}^{N-1} J_j^2,
\end{aligned} \tag{9}$$

where $\Phi(x) = (x-1)^2$ and $h^{(\mu)} = \sum_{j=1}^{N-1} J_j s_j^{(\mu)}$. Then, the Gibbs-Boltzmann distribution of the

student couplings is defined as

$$P\left(\boldsymbol{J}|\mathcal{D}^M\right) = \frac{1}{Z}\exp\left[-\beta\mathcal{H}\left(\boldsymbol{J}|\mathcal{D}^M\right)\right], \tag{10}$$

where β represents the inverse temperature and Z is the partition function

$$Z = \int d\boldsymbol{J}\exp\left[-\beta\mathcal{H}\left(\boldsymbol{J}|\mathcal{D}^M\right)\right]. \tag{11}$$

The Gibbs-Boltzmann distribution becomes the point-wise measure on the solution of (5) in the zero-temperature limit $\beta \to +\infty$, meaning that we can extract any information of the estimator from the Gibbs-Boltzmann distribution or the free energy. Hence, we concentrate on computing the free energy in the zero-temperature limit in the following. The free energy density averaged over the dataset is given by

$$f = -\frac{1}{N\beta}\left[\log Z\right]_{\mathcal{D}^M}. \tag{12}$$

Unfortunately, the average over the dataset of $\log Z$ is analytically difficult. To overcome this, we use the replica method from the statistical mechanics of disordered systems [16, 17, 18] as

$$f = -\frac{1}{N\beta}\left[\log Z\right]_{\mathcal{D}^M} = -\lim_{n\to 0}\frac{1}{N\beta}\frac{\partial}{\partial n}\log\left[Z^n\right]_{\mathcal{D}^M}, \tag{13}$$

$$\left[Z^n\right]_{\mathcal{D}^M} = \int\prod_{a=1}^{n} d\boldsymbol{J}^a e^{-\beta\lambda N\sum_{a=1}^{n}\|\boldsymbol{J}^a\|_2^2}\left\{\sum_{\boldsymbol{s}} P_{\text{Ising}}\left(\boldsymbol{s}|\boldsymbol{J}^*\right)\exp\left[-\beta\sum_{a=1}^{n}\Phi\left(s_0 h^a\right)\right]\right\}^{\alpha N}, \tag{14}$$

where $P_{\text{Ising}}\left(\boldsymbol{s}|\boldsymbol{J}^*\right)$ is the Boltzmann distribution of the teacher network in (1) with $\boldsymbol{H}^* = 0$ and the so-called cavity field is introduced:

$$h^a = \sum_{j=1}^{N-1} J_j^a s_j. \tag{15}$$

According to the standard prescription of the replica method, in eq. (14) we assumed $n \in \mathbb{N}$ to proceed with the calculation. The limit $n \to 0$ in eq. (13) is taken by using an analytical continuation of this expression at the end. To find such an expression is the task below.

3.1 Ansatz For Handling Cavity Fields

To calculate the integration in (14), we resort to the cavity approach used in [5, 6]. As the case of [6], the cavity field $h^a = \sum_j J_j^a s_j$ obeys a nontrivial distribution in the present case. To address this problem, we propose an ansatz which is a generalization of the one used in [6]. The generalized ansatz enables us to systematically treat the estimation bias on the coupling estimates in the inactive set $\{i|J_i^* = 0, i \in \{1,\cdots,N-1\}\}$. Such biases are absent in [6] but present in our case due to the ℓ_2 regularization we employ. In this subsection the details of the generalized ansatz are explained.

The basic idea of the ansatz is to categorize the estimators based on the distance or generation

from the focused spin s_0. If we consider a teacher Ising model whose coupling network takes a tree-like graph, we can naturally define generations of the spins according to the distance from the focused spin s_0. We categorize the spins directly connected to s_0 as the first generation and denote the corresponding index set as $\Omega_1 = \{i | J_i^* \neq 0, i \in \{1, \ldots, N-1\}\}$. Each spin in Ω_1 is connected to some other spins except for s_0, and those spins constitute the second generation and we denote its index set as Ω_2. This recursive construction of generations can be unambiguously continued on the tree-like graph, and we denote the index set of the d-th generation from spin s_0 as Ω_d. The overall construction of generations is graphically represented in Fig. 1.

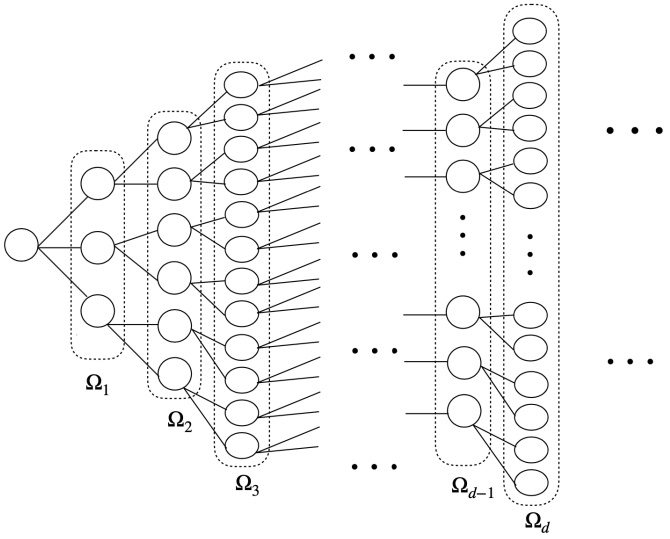


Figure 1: Schematic of generations of spins. In general, the d-th generation of spin s_0 is denoted as Ω_d, whose distance from spin s_0 is d.

Let us state our ansatz using the above definitions and notations. We introduce $\Psi_d = \{\Omega_1, \Omega_2 \ldots, \Omega_d\}$ and call it the nearest neighbors (NN) set of d generations. Our ansatz assumes that the estimates $\hat{\boldsymbol{J}} = \left(\hat{J}_i\right)_{i=1}^{N-1}$ obey the following form:

$$\hat{J}_i = \begin{cases} \bar{J}_i + \frac{1}{\sqrt{N}}\Delta_i, & i \in \Psi_d, \\ \frac{1}{\sqrt{N}}\Delta_i, & i \in \bar{\Psi}_d, \end{cases} \tag{16}$$

where $\bar{\Psi}_d$ denotes the complement set of Ψ_d and Δ_i is a random variable whose mean and variance are zero and $\mathcal{O}(1)$, respectively. The variance of the estimator corresponds to the variance of $\Delta_i/\sqrt{N}$, and thus it shrinks in the scaling $\mathcal{O}(1/N)$ in the large N limit. This is important for structure learning as later mentioned in Section 4. We call $\{\bar{J}_i\}_{i\in\Psi_d}$ mean estimates which are determined by minimizing the free energy. In this sense, the mean estimates can be considered as order parameters. Meanwhile, $\{\Delta_i\}_i$ are termed noise variables and also are integration variables which replace the ones in (14). If the estimation bias is absent in the inactive set $\bar{\Omega}_1$, then $d = 1$ is sufficient to take into account all the non-zero means in the estimators and thus is exact.

This is the case in the earlier study [6]. In the present case, however, the estimation bias exists also in the inactive set and hence we need larger values of d. In general, we can expect that the approximation of the free energy will be more accurate as d grows, but it involves the exponential increase of the number of the order parameter $\{\bar{J}_i\}_{i\in\Psi_d}$. Fortunately, as we see later, some small values of d, say $d=2$, provide a large improvement from $d=1$ and a quantitatively satisfactory result. This good nature comes from the fact that the absolute values of the mean estimates $\{\bar{J}_i\}_{i\in\Psi_d}$ decay exponentially fast as d increases, which is proved in Section 3.4 in the framework of the replica method. In this way we can provide an accurate ansatz to handle the integration in (14). The calculation details will be shown in the next subsections, and in the remaining part of this subsection we discuss some consequences of the ansatz.

Based on (16), the cavity field $h^a = \sum_j J_j^a s_j$ can be decomposed into the sum of the "signal" part h_{Ψ_d} and the "noise" part $h_\triangle^a$ as

$$h^a = h_{\Psi_d} + h_\triangle^a, \tag{17}$$

$$h_{\Psi_d} \doteq \sum_{j\in\Psi_d} \bar{J}_j s_j, \tag{18}$$

$$h_\triangle^a \doteq \frac{1}{\sqrt{N}} \sum_j \Delta_j^a s_j \approx \frac{1}{\sqrt{N}} \sum_{j\in\bar{\Psi}_d} \Delta_j^a s_j, \tag{19}$$

where the approximation in (19) is due to the assumption that there are only finite $\mathcal{O}(1)$ terms in Ψ_d, which are negligible in the large system limit, as discussed in Section 3.4. An important consequence of this decomposition is that the signal and noise parts are asymptotically independent as N grows against fixed d. This is because as N grows the majority of spins in the noise part become farer and farer from the spins in the NN set Ψ_d, and resultantly the dependence vanishes in the limit $N\to\infty$. This asymptotic independence makes the computation feasible in the next subsection.

Moreover, the ℓ_2 norm square of $\boldsymbol{J}^a = \left(J_j^a\right)_j$ can be computed as

$$\begin{aligned}\|\boldsymbol{J}^a\|^2 &= \sum_{j\in\Psi_d} \left(\bar{J}_j^2 + 2\bar{J}_j \frac{\Delta_j^a}{\sqrt{N}} + \frac{(\Delta_j^a)^2}{N} \right) + \frac{1}{N} \sum_{j\in\bar{\Psi}_d} \left(\Delta_j^a\right)^2 \\ &\approx \sum_{j\in\Psi_d} \bar{J}_j^2 + \frac{1}{N} \left\|\boldsymbol{\Delta}^a\right\|_2^2, \end{aligned} \tag{20}$$

where the summation of the noise terms over Ψ_d is ignored in the large system limit, which is again due to the assumption of $\mathcal{O}(1)$ terms in Ψ_d. Hence the signal and noise parts are decoupled again in the regularization term.

The RSS in (7) also takes a simple form:

$$\mathcal{E} \approx \sum_{j\in\Omega_1} \left| J_j^* - \bar{J}_j \right|^2 + \sum_{j\in\Psi_d\backslash\Omega_1} \bar{J}_j^2 + R, \tag{21}$$

where $\Psi_d\backslash\Omega_1$ denotes the NN set Ψ_d excluding Ω_1, and a macroscopic parameter R is introduced

as

$$R = \frac{1}{N} \sum_{j \in \bar{\Psi}_d} \triangle_j^2, \tag{22}$$

which indicates the sum of square errors in the set $\bar{\Psi}_d$ and is computed below.

3.2 Free Energy Density

Following the ansatz in Section 3.1, we can rewrite the replicated partition function $[Z^n]_{\mathcal{D}^M}$ of (14) as written as

$$\begin{aligned}
[Z^n]_{\mathcal{D}^M} &= \int \prod_{a=1}^{n} d\boldsymbol{J}^a e^{-\lambda\beta N \sum_{a=1}^{n} \|\boldsymbol{J}^a\|^2} \left\{ \sum_{\boldsymbol{s}} P_{\text{Ising}}\left(\boldsymbol{s}|\boldsymbol{J}^*\right) \exp\left[-\beta \sum_{a=1}^{n} \Phi\left(s_0 h^a\right) \right] \right\}^{\alpha N} \\
&\approx \int \prod_{a=1}^{n} d\boldsymbol{\Delta}^a e^{-\lambda\beta\left(Nn \sum_{j \in \Psi_d} \bar{J}_j^2 + \sum_{a=1}^{n} \|\boldsymbol{\Delta}^a\|^2 \right)} \times \\
&\quad \left\{ \sum_{\boldsymbol{s}} P_{\text{Ising}}\left(\boldsymbol{s}|\boldsymbol{J}^*\right) \prod_{a} \int dh_{\triangle}^a \delta\left(h_{\triangle}^a - \frac{1}{\sqrt{N}} \sum_{j \in \bar{\Psi}_d} \Delta_j^a sj \right) e^{-\beta \sum_{a=1}^{n} \Phi\left(s_0 \left(\sum_{j \in \Psi_d} \bar{J}_j s_j + h_{\triangle}^a \right) \right)} \right\}^{\alpha N} \\
&= \int \prod_{a=1}^{n} d\boldsymbol{\Delta}^a e^{-\lambda\beta\left(Nn \sum_{j \in \Psi_d} \bar{J}_j^2 + \sum_{a=1}^{n} \|\boldsymbol{\Delta}^a\|^2 \right)} \times \\
&\quad \left\{ \sum_{s_0, \boldsymbol{s}_{\Psi_d}} P\left(s_0, \boldsymbol{s}_{\Psi_d}, \left\{ h_{\triangle}^a \right\}_a | J^*, \left\{ \boldsymbol{\Delta}^a \right\}_a \right) e^{-\beta \sum_{a=1}^{n} \Phi\left(s_0 \left(\sum_{j \in \Psi_d} \bar{J}_j s_j + h_{\triangle}^a \right) \right)} \right\}^{\alpha N} \\
&\approx \int \prod_{a=1}^{n} d\boldsymbol{\Delta}^a e^{-\lambda\beta\left(Nn \sum_{j \in \Psi_d} \bar{J}_j^2 + \sum_{a=1}^{n} \|\boldsymbol{\Delta}^a\|^2 \right)} \times \\
&\quad \left\{ \sum_{s_0, \boldsymbol{s}_{\Psi_d}} P\left(s_0, \boldsymbol{s}_{\Psi_d} | J^* \right) \int \prod_{a=1}^{n} dh_{\triangle}^a P_{\text{cav}}\left(\left\{ h_{\triangle}^a \right\}_a | \left\{ \boldsymbol{\Delta}^a \right\}_a \right) e^{-\beta \sum_{a=1}^{n} \Phi\left(s_0 \left(\sum_{j \in \Psi_d} \bar{J}_j s_j + h_{\triangle}^a \right) \right)} \right\}^{\alpha N},
\end{aligned} \tag{23}$$

where $\boldsymbol{s}_{\Psi_d}$ is the vector of spins in the NN set Ψ_d. In the second line of (23), $\sum_{j \in \Psi_d} \left(\Delta_j^a \right)^2$ is ignored as in (20), and in the last line, the asymptotic independence between $h_{\triangle}^a$ and $\{s_0, \boldsymbol{s}_{\Psi_d}\}$ are used. The marginal distribution $P\left(s_0, \boldsymbol{s}_{\Psi_d} | J^*\right)$ is computed by marginalizing the whole distribution $\sum_{\boldsymbol{s}} P_{\text{Ising}}\left(\boldsymbol{s}|\boldsymbol{J}^*\right)$ with respect to $\boldsymbol{s}_{\bar{\Psi}_d}$, which can be obtained as

$$P\left(s_0, \boldsymbol{s}_{\Psi_d} | J^*\right) = \sum_{\boldsymbol{s}_{\bar{\Psi}_d}} P\left(\boldsymbol{s}|J^*\right). \tag{24}$$

Then, according to the central limit theorem, the noise part $\left\{ h_{\triangle}^a \right\}_{a=1}^{n}$ can be regarded as Gaussian variables so that the cavity distribution $P_{\text{cav}}\left(\left\{ h_{\triangle}^a \right\}_a | \left\{ \boldsymbol{\Delta}^a \right\}_a \right)$ can be assumed as a multivariate Gaussian distribution. Here we assume the replica symmetry (RS), and hence the following two order parameters are sufficient to characterize the multivariate Gaussian

distribution:

$$Q \doteq \frac{1}{N} \sum_{i,j \in \bar{\Psi}_d} \Delta_i^a C_{ij}^{\backslash 0} \Delta_j^a, \tag{25}$$

$$q \doteq \frac{1}{N} \sum_{i,j \in \bar{\Psi}_d} \Delta_i^a C_{ij}^{\backslash 0} \Delta_j^b, \ (a \neq b), \tag{26}$$

where $\boldsymbol{C}^{\backslash 0} = \left(C_{ij}^{\backslash 0}\right)_{ij}$ is the correlation matrix of the reduced spin system without s_0. As suggested in [5, 6], the non-diagonal elements of $\boldsymbol{C}^{\backslash 0}$ will have a nontrivial contribution and will hence be retained. To write the integration in terms of the order parameters Q, q, we introduce the following trivial identities:

$$1 = N \int dQ \ \delta \left(\sum_{i,j \neq 0} \Delta_i^a C_{ij}^{\backslash 0} \Delta_j^a - NQ \right), a = 1, ..., n, \tag{27}$$

$$1 = N \int dq \ \delta \left(\sum_{i,j \neq 0} \Delta_i^a C_{ij}^{\backslash 0} \Delta_j^b - Nq \right), a < b, a, b \neq *. \tag{28}$$

Therefore, $[Z^n]_{\mathcal{D}^M}$ can be rewritten as

$$\begin{aligned}
&[Z^n]_{\mathcal{D}^M} = e^{-\lambda\beta Nn \sum_{j\in\Psi_d} \bar{J}_j^2} \int dQdq \int \prod_{a=1}^{n} d\boldsymbol{\Delta}^a e^{-\lambda\beta \sum_{a=1}^{n} \|\boldsymbol{\Delta}^a\|^2} \prod_{a=1}^{n} \delta \left(\sum_{i,j} \Delta_i^a C_{ij}^{\backslash 0} \Delta_j^a - NQ \right) \times \\
&\prod_{a<b} \delta \left(\sum_{i,j} \Delta_i^a C_{ij}^{\backslash 0} \Delta_j^b - Nq \right) \times \\
&\left\{ \sum_{s_0, \boldsymbol{s}_{\Psi_d}} P\left(s_0, \boldsymbol{s}_{\Psi_d} | J^*\right) \int \prod_{a=1}^{n} dh_{\triangle}^a P_{\text{cav}} \left(\left\{ h_{\triangle}^a \right\}_a | \left\{ \boldsymbol{\Delta}^a \right\}_a \right) e^{-\beta \sum_{a=1}^{n} \Phi\left(s_0 \left(\sum_{j\in\Psi_d} \bar{J}_j s_j + h_{\triangle}^a \right) \right)} \right\}^{\alpha N} \\
&= \int dQdq \exp\left[NS + \alpha N \log L \right],
\end{aligned} \tag{29}$$

where

$$\begin{aligned}
e^{NS} \doteq & e^{-\lambda\beta Nn \sum_{j\in\Psi_d} \bar{J}_j^2} \int \prod_{a=1}^{n} d\boldsymbol{\Delta}^a e^{-\lambda\beta \sum_{a=1}^{n} \|\boldsymbol{\Delta}^a\|^2} \prod_{a=1}^{n} \delta \left(\sum_{i,j} \Delta_i^a C_{ij}^{\backslash 0} \Delta_j^a - NQ \right) \\
& \times \prod_{a<b} \delta \left(\sum_{i,j} \Delta_i^a C_{ij}^{\backslash 0} \Delta_j^b - Nq \right),
\end{aligned} \tag{30}$$

$$L \doteq \sum_{s_0, \boldsymbol{s}_{\Psi_d}} P\left(s_0, \boldsymbol{s}_{\Psi_d} | J^*\right) \int \prod_{a=1}^{n} dh_{\triangle}^a P_{\text{cav}} \left(\left\{ h_{\triangle}^a \right\}_a | \left\{ \boldsymbol{\Delta}^a \right\}_a \right) e^{-\beta \sum_{a=1}^{n} \Phi\left(s_0 \left(\sum_{j\in\Psi_d} \bar{J}_j s_j + h_{\triangle}^a \right) \right)}. \tag{31}$$

After performing some algebraic operations presented in Appendix A and Appendix B, we obtain the results in the limit $n \to 0$:

$$\lim_{n\to 0} \frac{S}{n} = -\lambda\beta \sum_{j\in\Psi_d} \bar{J}_j^2 + \frac{Q\beta}{2} G_1^{-1}\left(\beta\left(Q-q\right)\right) - \frac{1}{2} G_2\left(G_1^{-1}\left(\beta\left(Q-q\right)\right)\right) + \frac{1}{2}\log\frac{2\pi}{\beta} - \frac{1}{2N}\mathrm{Tr}\log\left(\boldsymbol{C}^{\backslash 0}\right)^{-1}, \tag{32}$$

$$\lim_{n\to 0} \frac{1}{n}\log L = \sum_{s_0, \boldsymbol{s}_{\Psi_d}} P\left(s_0, \boldsymbol{s}_{\Psi_d}|J^*\right) \int \mathcal{D}z \log \int \mathcal{D}v e^{-\beta\sum_{a=1}^{n}\Phi\left(s_0\left(\sum_{j\in\Psi_d}\bar{J}_j s_j + \sqrt{Q-q}v + \sqrt{q}z\right)\right)}, \tag{33}$$

where $\mathcal{D}z = \frac{dz}{\sqrt{2\pi}} e^{-\frac{z^2}{2}}$, and

$$G_1\left(x\right) = \int d\eta \frac{\rho\left(\eta\right)}{x + 2\lambda\eta}, \tag{34}$$

$$G_2\left(x\right) = \int d\eta \rho\left(\eta\right) \log\left(x + 2\lambda\eta\right), \tag{35}$$

where $\rho\left(\eta\right)$ is the eigenvalue distribution (EVD) of the inverse correlation matrix, i.e., $\left(\boldsymbol{C}^{\backslash 0}\right)^{-1}$, as shown in Appendix E. Note that G_1^{-1} denotes the inverse function of G_1, i.e., $x = G_1^{-1}\left(y\right)$ implies that $y = G_1\left(x\right)$. In the special case of $\lambda = 0$, $G_1\left(x\right) = 1/x$ and $G_1^{-1}\left(y\right) = 1/y$.

Further, we take the limit $\beta \to \infty$, which requires the following relation [5, 6]:

$$\lim_{\beta\to\infty} \beta\left(Q-q\right) = \chi = \mathcal{O}\left(1\right). \tag{36}$$

$\chi = \mathcal{O}\left(1\right)$ is a finite number, and according to (34), $G_1^{-1}\left(\beta\left(Q-q\right)\right)$ should also be a finite number. Then, denoting $G_1^{-1}\left(\beta\left(Q-q\right)\right) \doteq \kappa$, after performing some algebraic operations, we obtain the free energy density (13) in the limit $\beta \to \infty$ as

$$f\left(\beta\to\infty\right) = -\underset{Q,\kappa,\{\bar{J}_j\}_{j\in\Psi_d}}{\mathrm{Extr}} \left\{ -\lambda \sum_{j\in\Psi_d} \bar{J}_j^2 + \frac{Q}{2}\kappa + \alpha \sum_{s_0, \boldsymbol{s}_{\Psi_d}} P\left(s_0, \boldsymbol{s}_{\Psi_d}|J^*\right) \int \mathcal{D}z \max_y \left[-\frac{\left(y - s_0\left(\sqrt{Q}z + \sum_{j\in\Psi_d}\bar{J}_j s_j\right)\right)^2}{2G_1\left(\kappa\right)} - \Phi\left(y\right) \right] \right\}, \tag{37}$$

where $\underset{x}{\mathrm{Extr}}\left\{\cdot\right\}$ denotes extremization w.r.t. x.

3.3 Equations of State (EOS)

From (37), the extremization condition leads to the following equations of state (EOS):

$$\kappa - \frac{\alpha}{\sqrt{Q}} \int \mathcal{D}z z \frac{\partial l\left(y\right)}{\partial y} \mid_{y=\hat{y}} = 0, \tag{38}$$

$$Q + \alpha G_1^{'}\left(\kappa\right) \int \mathcal{D}z \left(\frac{\partial l\left(y\right)}{\partial y} \mid_{y=\hat{y}} \right)^2 = 0, \tag{39}$$

where

$$\hat{y} = \arg\max_{y} \left(- \frac{\left(y - s_0 \left(\sqrt{Q} z + \sum_{j \in \Psi_d} \bar{J}_j s_j \right) \right)^2}{2 G_1\left(\kappa\right)} - \Phi\left(y\right) \right). \tag{40}$$

Moreover, the mean estimates $\left\{ \bar{J}_j \right\}_{j \in \Psi_d}$ can also be evaluated by the extremization condition, i.e.,

$$0 = 2\lambda \bar{J}_j + \alpha \sum_{s_0, \boldsymbol{s}_{\Psi_d}} P\left(s_0, \boldsymbol{s}_{\Psi_d} | J^*\right) \int \mathcal{D}z \frac{\partial \Phi\left(y\right)}{\partial y} \mid_{y=\hat{y}} s_0 s_j, \ j \in \Psi_d, \tag{41}$$

which is a set of linear equations in our case of the quadratic cost function. Note that when the coupling strength is uniform, i.e., $\left| J_j^* \right| = K, \ j \in \Omega_1$, the strength of the mean estimates $\bar{J}_j \in \Omega_1$ can also be set to a uniform value $\left| \bar{J}_j \right| = \bar{K} = \hat{b} K$, where the bias factor is defined as

$$\hat{b} \doteq \frac{\bar{K}}{K}. \tag{42}$$

Besides, using the auxiliary variable technique similar to [6], as shown in Appendix C, the macroscopic parameter R in (22) can be computed as

$$R = \frac{1}{N} \sum_{j \in \bar{\Psi}_d} \triangle_j^2 = q \frac{G_3^{'}\left(\kappa\right)}{G_1^{'}\left(\kappa\right)}, \tag{43}$$

where

$$G_3\left(x\right) = \int d\eta \frac{\rho\left(\eta\right)\eta}{\left(x + 2\lambda\eta\right)}, \tag{44}$$

and $G_1^{'}\left(x\right)$ and $G_3^{'}\left(x\right)$ are the first-order derivatives of $G_1\left(x\right)$ and $G_3\left(x\right)$, respectively. Then, given $\left\{ \bar{J}_j \right\}_{j \in \Psi_d}$, Q, κ, the RSS in (7) can be computed as

$$\mathcal{E} \approx \sum_{j \in \Omega_1} \left| J_j^* - \bar{J}_j \right|^2 + \sum_{j \in \Psi_d \backslash \Omega_1} \bar{J}_j^2 + Q \frac{G_3^{'}\left(\kappa\right)}{G_1^{'}\left(\kappa\right)}. \tag{45}$$

In general, no analytical solution exists for the EOS, but it can be easily solved using numerical methods, as illustrated in Appendix D.

3.4 Nearest-Neighbor Effect

In this subsection, we study the NN effect by examining the mean estimates $\left\{\bar{J}_j\right\}_{j\in\Psi_d}$, and the application range of ansatz (16) is also discussed. According to the replica analysis presented above, the mean estimates $\left\{\bar{J}_j\right\}_{j\in\Psi_d}$ can be calculated by solving the linear equations

$$(1+2\lambda/\kappa)\,\bar{J}_j+\sum_{i\in\Psi_d,i\neq j}\bar{J}_i\,\langle s_i s_j\rangle-\langle s_0 s_j\rangle=0,\ j\in\Psi_d, \tag{46}$$

where $\langle s_i s_j\rangle$ is the correlation function w.r.t. the joint distribution $P\left(s_0,\boldsymbol{s}_{\Psi_d}|J^*\right)$. First, consider the special case without regularization. The result is given in Theorem 1.

Theorem 1. *For a teacher Ising model with a sparse tree-like coupling network in the paramagnet phase, using linear regression without regularization, the mean estimates* $\left\{\bar{J}_j\right\}_{j\in\Psi_d}$ *in (46) are*

$$\bar{J}_j=\begin{cases}\frac{1}{\sum_{k\in\Omega_1}\frac{1}{1-\tanh^2 J_k^*}-c+1}\cdot\frac{\tanh(J_j^*)}{1-\tanh^2(J_j^*)} & j\in\Omega_1\\ 0, & j\notin\Omega_1\end{cases}, \tag{47}$$

where c is the number of first-generation nearest neighbors of s_0, i.e., $c=|\Omega_1|$. In particular, with uniform coupling, i.e., $\left|J_j^*\right|=K, j\in\Omega_1$, it is

$$\bar{J}_j=\begin{cases}\frac{\tanh K}{1+(c-1)\tanh^2 K}\mathrm{sign}(J_j^*), & j\in\Omega_1\\ 0, & j\notin\Omega_1\end{cases}. \tag{48}$$

The proof is given in Appendix F. Theorem 1 shows that, even under model mismatch, naive linear regression without regularization can reconstruct the active set Ω_1, i.e., $\bar{J}_j=0, j\in\Psi_d\backslash\Omega_1$. This result is consistent with the result in [6], which is obtained by analyzing the zero-gradient condition for the general loss function. Consequently, when $\lambda=0$, we can simply ignore the biases $\bar{J}_j, j\notin\Omega_1$ of the estimator when computing the RSS in (45).

However, when there is regularization, the result is different, as stated in Theorem 2.

Theorem 2. *For a teacher Ising model of uniform coupling strength K with a sparse tree-like coupling network in the paramagnet phase, using ℓ_2-regularized linear regression with regularization coefficient $\lambda>0$, the mean estimates* $\left\{\bar{J}_j\right\}_{j\in\Psi_d}$ *in (46) are biased to nonzero values in the inactive set but decay at least exponentially fast w.r.t. the distance from spin s_0 with factor $\delta=\theta\frac{(D-1)}{D-\theta^2}$, where $D=1+\frac{2\lambda}{\kappa}$ and $\theta=\tanh K$.*

The proof is given in Appendix G. Theorem 2 shows that the use of ℓ_2 regularization in ridge regression introduces biases into the coupling estimates for the inactive set; hence, one must be careful about the potential false positives when using ℓ_2 regularization. The biases decay at least exponentially fast w.r.t. the distance d between s_j and s_0. Namely, the relation $\left|\bar{J}_j/\bar{J}_k\right|<\delta^{d-1}$ holds for $\forall j\in\Omega_d$ and the j's ascendant $k\in\Omega_1$. Thus, despite the nonzero biases in the inactive set, the ansatz (16) provides an accurate approximation even if we only consider small finite

values of d. This result holds for any tree graph, and also applies if the graph is asymptotically tree-like in the large system limit.

This result can be seen from another perspective. Let us consider a RR graph with uniform coupling strength K. The above upper bound to the coupling estimates implies that the bias's total contribution of the d-th generation Ω_d to the RSS is also upper bounded as

$$\sum_{j\in\Omega_d} \bar{J}_j^2 < c\,(c-1)^{d-1}\left[\tanh^2(K)\right]^{d-1}\bar{K}_{\Omega_1}^2, \tag{49}$$

where we use an inequality $\delta = \theta(D-1)/(D-\theta) < \theta = \tanh K$ and denote $\bar{K}_{\Omega_1}$ as the absolute value of the mean estimates in Ω_1. Thus, from (49), as long as $(c-1)\tanh^2 K < 1$, this bias contribution converges to zero as d grows and thus can be ignored when d is large enough. Interestingly, the paramagnetic condition $(c-1)\tanh^2 K < 1$ [6, 16, 17] corresponds to this converging condition.

4 Structure Learning and Two-Stage Estimator

From the analysis presented in Section 3, for naive linear regression without regularization, the estimates in the inactive set $\hat{J}_j \sim \mathcal{O}(1/\sqrt{N}),\ j \notin \Omega_1$ are unbiased. Since the variance of estimator scales as $\mathcal{O}(1/N)$, which is later demonstrated when comparing the theoretical result and numerical experiment, we can obtain the perfect recovery in the limit $N \to \infty$ by pruning the estimates with an appropriate threshold $K_{\rm th}(>0)$. It is also possible to show that the probability of successfully screening out false positives approaches one by following the same argument as [6]. Hence, the structure learning is perfectly achievable in the case without regularization.

Unfortunately, the naive linear regression is only applicable to the $\alpha > 1$ case, and for the underdetermined region $\alpha < 1$ the regularization is needed. However, the use of ℓ_2 regularization leads to non-zero biases in the inactive set as stated in Theorem 2, which makes the above pruning method difficult to be successful. To overcome this difficulty, based on the other observation in Theorem 2 that the biases decay at least exponentially fast w.r.t. the distance, we propose a two-stage estimator which combines the advantages of both naive linear regression and ℓ_2-regularized linear regression.

The specific procedures of the two-stage estimator are as follows. In the first stage, the ℓ_2-regularized linear regression is applied and the resultant estimate is denoted as $\hat{\boldsymbol{J}}^{\rm stg1}$. To control false positives, a certain constant threshold value $K_1(\sim\mathcal{O}(1))$ is introduced, and the elements of $\hat{\boldsymbol{J}}^{\rm stg1}$ whose absolute values are less than K_1 are considered as negligible and set to zero, i.e.,

$$\hat{J}_j^{\text{stg1-th}} = \begin{cases} \hat{J}_j^{\rm stg1}, & \text{if } \left|\hat{J}_j^{\rm stg1}\right| > K_1, \\ 0, & \text{otherwise.} \end{cases} \tag{50}$$

In contrast to the above pruning method, the threshold K_1 is not required to eliminate all the false positives, but it should be sufficiently small to avoid false negatives, which is relatively easy to implement. According to Theorem 2, the biases in the inactive set decay exponentially

fast and hence there will be only $\mathcal{O}(1)$ false positives in $\hat{\boldsymbol{J}}^{\text{stg1-th}}$. To further eliminate those $\mathcal{O}(1)$ false positives, in the second stage, the naive linear regression without regularization is applied only to the support of $\hat{\boldsymbol{J}}^{\text{stg1-th}}$, which leads to another estimate $\hat{\boldsymbol{J}}^{\text{stg2}}$. We again prune this estimate by introducing another threshold $K_2(\sim \mathcal{O}(1))$, which corresponds to K_{th} in the single-step pruning method, to judge the estimate component satisfying $|\hat{J}_j^{\text{stg2}}| < K_2$ as zero. Since there are only $\mathcal{O}(1)$ false positives after the first stage, the problem in the second stage effectively corresponds to the situation $\alpha \to \infty$ ($\mathcal{O}(1)$ unknowns but with $M = \alpha N \to \infty$ samples) in the large system limit; hence, the perfect recovery is again possible. These procures provide a practical and reasonable way to achieve the perfect recovery for all $\alpha > 0$. We could thus derive the positive answer to the structure learning for inverse Ising problems even in the model mismatch setting.

In the next section, the effectiveness of the above proposed method is demonstrated in numerical experiments, to show a quantitatively satisfactory performance.

5 Numerical experiments

Here we conduct numerical experiments to examine the theoretical analysis and the performance of the proposed estimators. The experimental setup is as follows. The teacher Ising model is assumed to have a uniform coupling strength K, and the coupling network is assumed to be the RR graph with a connectivity parameter c or the ER graph with the connection probability p. As in [6], to keep the generated graph sufficiently sparse in the ER case, the probability p is assumed to scale as $p = \bar{c}/N$, yielding the mean degree $\bar{c}$. We assume that the active couplings of the teacher model have the same probability of taking both signs. In addition, K is assumed to be sufficiently small to satisfy the paramagnet assumption of the teacher model [6, 16, 17]. The experimental procedures are similar to those in [6]. First, a random graph is generated and the teacher Ising model with coupling strength K is defined on it. From the teacher model, the spin snapshots are obtained using MC sampling, yielding the dataset $\mathcal{D}^M$. Then, we randomly choose a center spin s_0 from all the spins and infer the associated couplings connected to s_0 by applying our linear estimators to $\mathcal{D}^M$. The experimental values of the macroscopic quantities of interest, such as RSS, can be easily obtained. To obtain the error bars of them, we repeat the sequence of operations many times. Note that in the MC sampling, we started from a random initial configuration and updated the state by the standard Metropolis method; one MC step (MCS) is defined by N trial flips of spins, where N is the total number of spins. We discarded the first 10^5 MCSs as burn-in to avoid systematic errors from the initialization.

First, let us consider the case without regularization, i.e., $\lambda = 0$. Here, the NN set Ψ_d is fixed to be $\Psi_d = \Omega_1$ in the theoretical analysis, as the estimates are unbiased in the inactive set as stated in Theorem 1. The theoretical and experimental values of the RSS $\mathcal{E}$, order parameter Q, and bias factor $\hat{b}$ for the RR graph are shown in Fig. 2, where the error bars are obtained from 100 random runs. As can be seen from Fig. 2, the experimental and theoretical results are in fairly good agreement, which supports the validity of the theoretical analysis. The divergence of the RSS and Q at $\alpha \to 1$ corresponds to the phase transition when approaching to the

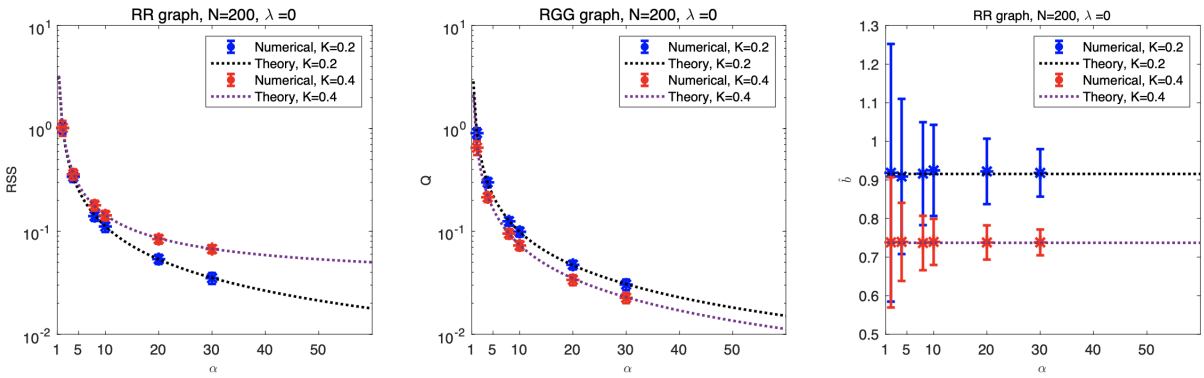


Figure 2: Plots of RSS $\mathcal{E}$, Q, and bias factor $\hat{b}$ for the RR graph with $(N, c) = (200, 3)$ for $K = 0.2, 0.4$ using linear regression, i.e., $\lambda = 0$. The dotted lines and colored markers represent the replica prediction and numerical values, respectively. The RSS and Q diverge in the limit $\alpha \to 1$. The error bars are obtained from 100 random runs.

underdetermined region $\alpha < 1$, signaling the limit of using the naive linear regression without regularization.

To see the structure learning performance, Fig. 3 shows the empirical values of Recall and Precision defined in eq. (8) for both the RR and ER graphs when $\alpha = 10$ (results with other values of $\alpha > 1$ are similar). Perfect recovery is achieved when both Recall and Precision are equal to 1, and we can see there exists a threshold interval actually realizing this. As N increases, this threshold interval becomes larger, and, as our theoretical analysis indicates, it should be $\left(0, \bar{K}_{\Omega_1}\right)$ in the large system limit, where $\bar{K}_{\Omega_1} = \min_{j \in \Omega_1} \left|\bar{J}_j\right|$ is the minimum mean estimate in the active set Ω_1. This sufficiently wide interval makes the use of naive linear regression practical.

Next, we turn to the finite regularization or the ridge regression case $\lambda > 0$. The theoretical and experimental values of the RSS $\mathcal{E}$, order parameter Q, and bias factor $\hat{b}$ for the RR graph are shown in Fig. 4. Compared to Fig. 2, there are three main differences. First, the use of ℓ_2 regularization successfully eliminates the divergence in the limit $\alpha \to 1$, making it applicable in the underdetermined region $\alpha < 1$. Second, the biases of the neighboring spins cannot always be ignored, especially when λ and/or K is large, as indicated by the lower part of Fig. 4, which shows the apparent discrepancy between the experimental results and the theoretical prediction when ignoring all the biases $\left\{\bar{J}_j\right\}_{j \in \Omega_d, d \geq 2}$. This implies that one must be careful about the potential false positives caused by the nonzero biases on the $d \geq 2$ generations when using ℓ_2-regularized linear regression. This is consistent with the result in Theorem 2: when λ and/or K is large, the decay factor $\delta = \theta \frac{(D-1)}{D-\theta^2}$ is high; hence, the biases in the inactive set decay slowly. Yet, owing to the exponential decay, it is considered to be possible to make a good approximation just by choosing some small value of d. Actually as shown in Fig. 4, putting $d = 2$ leads to fairly good agreement between the theoretical and experimental results. This can also be verified by empirically evaluating the distribution of estimates $\left\{\hat{J}_j\right\}$ in different Ω_d, which is shown in Fig. 5 for the first three generations. In the lower part of Fig. 5, when the regularization coefficient is $\lambda = 10$, the histograms of the inactive couplings in Ω_d with $d = 2$ are far from the zero-mean

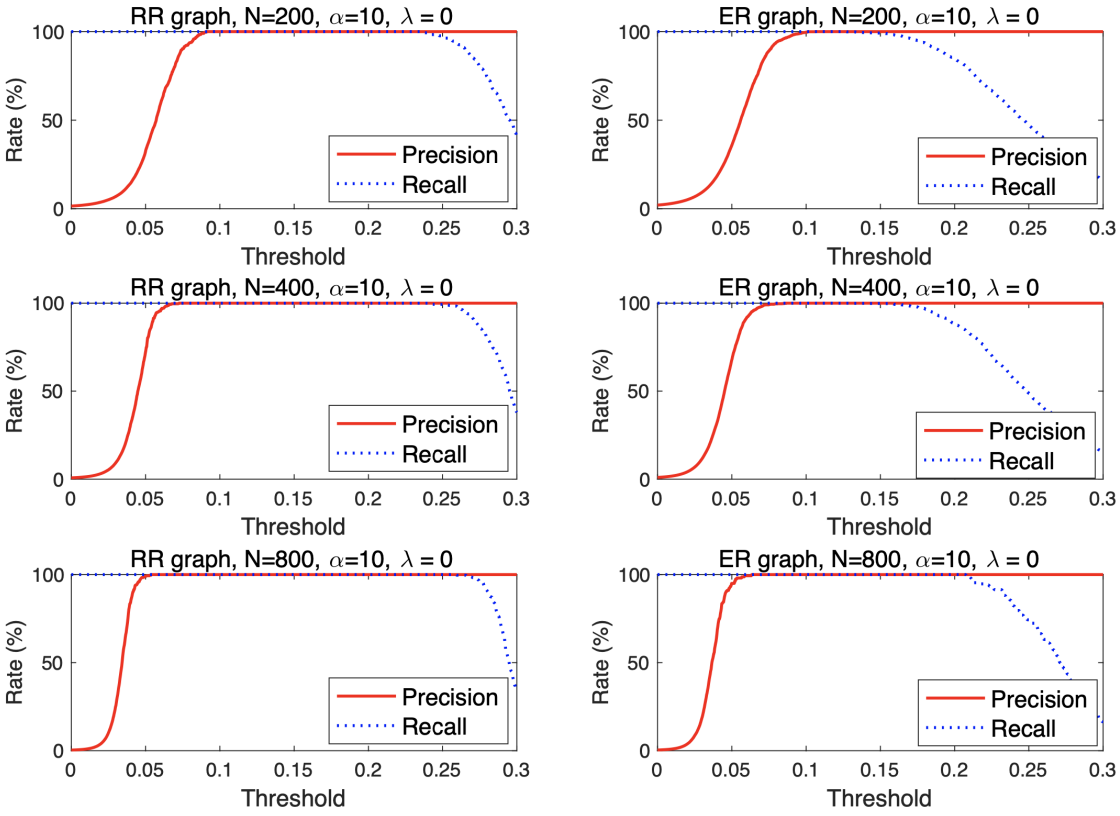


Figure 3: Precision and Recall plotted against the threshold $K_{\rm th}$ for RR and ER graphs using naive linear regression without regularization for different N in the case of $K = 0.4$ and $\alpha = 10$. For the RR graph, $c = 3$; for the ER graph, $\bar{c} = 4$. The dotted and solid lines represent Recall and Precision, respectively. Ten different ER graphs are generated, each with two independent MC samplings, and learning is then conducted for all $i = 0, ..., N-1$.

Gaussian. Therefore, in this case, apart from the true active set Ω_1, the NN spins in Ω_2 should also be considered as indicated in Fig. 4. The dashed straight line represents the mean estimates $\{\bar{J}_j\}$ with different distances d from s_0 computed from (41). When the regularization coefficient is small, e.g., $\lambda = 0.1$, the histograms of inactive couplings in Ω_d, $d \geq 2$ are similar to the zero-mean Gaussian; see the upper part of Fig. 5. In this case, ignoring the spins with $d \geq 2$ in the theoretical analysis still leads to good agreement with the experimental result as shown in Fig. 4. The last difference between ℓ_2-regularized linear regression and naive linear regression is that the bias factor $\hat{b}$ is not a constant; it increases as α increases and λ decreases.

Finally, the effectiveness of the proposed two-stage linear estimator for structure learning is evaluated in the case of the RR and ER graphs. Fig. 6 shows a typical result of the empirical Precision and Recall for the RR graph using the two-stage linear estimator with different N when $K = 0.4$, $\alpha = 0.8$, $\lambda = 0.1$. Perfect structure recovery can be achieved with a properly chosen threshold as N increases, e.g., as seen for $N = 800$ in Fig. 6, which verifies the analysis in Section 4. It is worth noting that, since the noise variance scales as $\mathcal{O}(1/N)$, the number of components beyond a certain threshold decreases as N increases, as shown in Fig. 7. This means

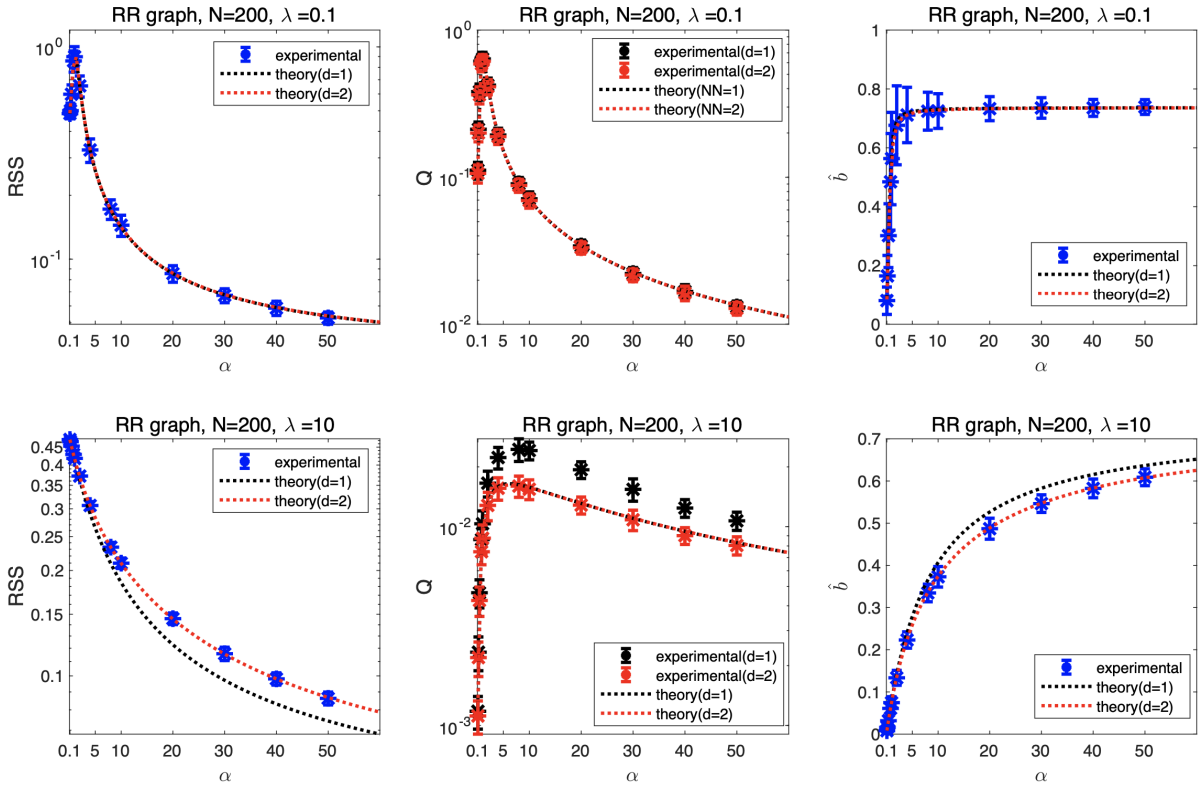


Figure 4: Plots of RSS $\mathcal{E}$, Q , and bias factor $\hat{b}$ for the RR graph with $(N, c) = (200, 3)$ with $K = 0.4$ using ridge regression with $\lambda = 0.1, 10$. The dotted lines and colored markers represent the replica prediction and numerical values, respectively. Note that the experimental values of Q are different for $d = 1$ and $d = 2$ since Q is related to the definition of Ψ_d, as shown in (25). The error bars are obtained from 100 random runs.

that as long as the threshold $K_1 \sim \mathcal{O}(1)$ is chosen to be sufficiently small to avoid ignoring true positives, the number of false positives after the first stage can be reduced to a certain $\mathcal{O}(1)$ value as $N \to \infty$. This effectively yields the asymptotic limit of $M \to \infty$ keeping N $\mathcal{O}(1)$; thus, one can easily distinguish true positives from false positives in the second stage. The validity of the two-stage estimator is also evaluated in the case of the ER graph with mean degree $\bar{c} = 4$ when $K = 0.4$, $\alpha = 0.9$, $\lambda = 0.1$, as shown in Fig. 8. Although the perfect recovery is not completely achieved (when $N = 1600$, there is a threshold interval where empirical Recall and Precision both achieve 99.90% simultaneously.) owing to the finite size effect, the empirical result in Fig. 8 indicates the tendency of improvement as N increases, which implies perfect recovery for $N \to \infty$. Note that in the case of the ER graph, we generated 10 different graphs, each with two independent MC samplings, and then conducted learning for all $i = 0, ..., N - 1$.

6 Summary and Discussion

In this paper, we theoretically investigated the performance of the ℓ_2- regularized linear estimator applied to the inverse Ising problem in the teacher-student scenario where the couplings of the

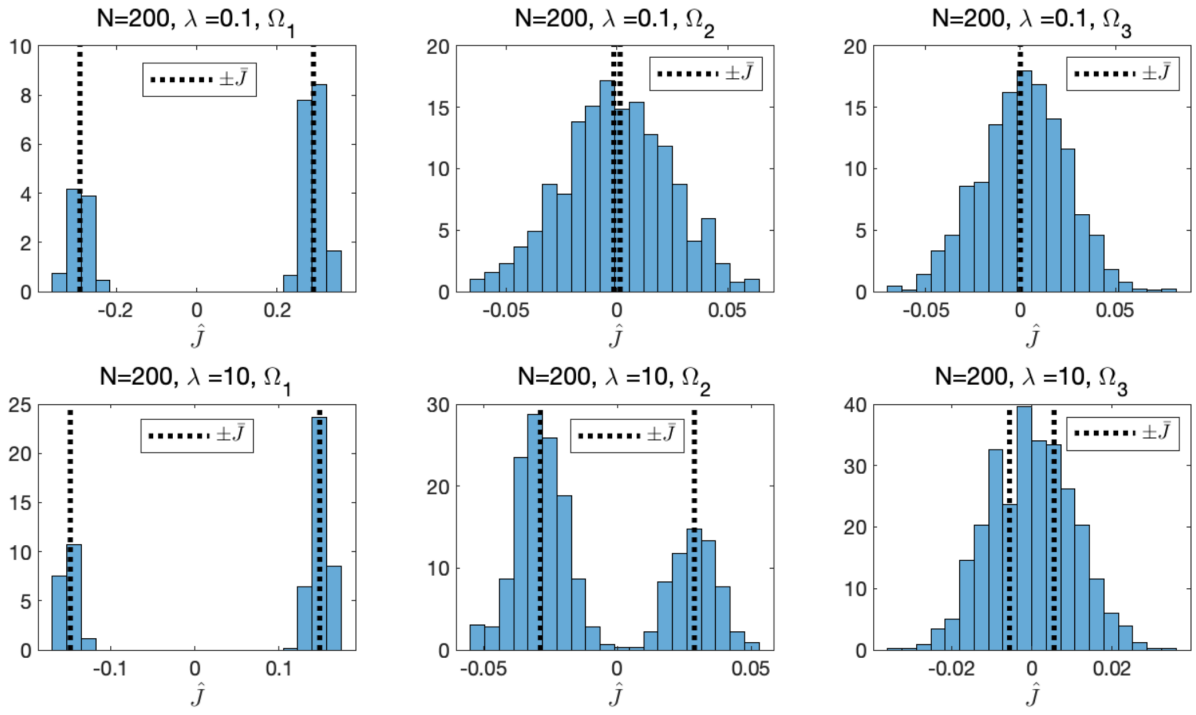


Figure 5: Histograms of the estimations $\hat{\boldsymbol{J}}$ in the first three generations $\Omega_d,\ d = 1, 2, 3$ from s_0. The system parameters are $(N, K, c, \alpha,) = (200, 400, 3, 10)$ with $\lambda = 0.1, 10$. The histograms are generated from 100 random runs. In contrast to linear regression, there are nonzero biases in the NN inactive spins $\Omega_d, d \geq 2$, which cannot always be ignored, especially when λ and/or K is large, e.g., the histograms of the inactive couplings in Ω_2 are far from the zero-mean Gaussian when $\lambda = 10$, as shown in the lower part.

teacher network are assumed to be sparse and the student has no prior knowledge of its structure and associated parameters, as a representative model mismatch situation. A special focus is on the reconstruction performance of the teacher coupling network. Using the replica and cavity methods of statistical mechanics, we showed that despite the model mismatch, one can perfectly reconstruct the network structure. This is naturally realized owing to the unbiasedness of the linear estimator in the inactive set when the regularization is absent, while it is efficiently achieved using the proposed two-stage estimator when the regularization is present. The proposed two-stage estimator is applicable even when the dataset size is smaller than the number of spins. The results of experiments conducted on locally tree-like graphs [**?**, **?**] verified the validity of both the theoretical analysis and the effectiveness of the linear estimator in structure learning in inverse Ising problems.

The two critical assumptions in this study are the ansatz for handling the cavity field (16) and the paramagnetic assumption for the teacher network. As discussed in Section 3.1, the ansatz holds for trees and asymptotic tree-like graphs. The paramagnetic assumption implies that the coupling strength should be sufficiently small. These assumptions restrict the applicability of the presented result, and thus overcoming such limitations will be an important direction for future

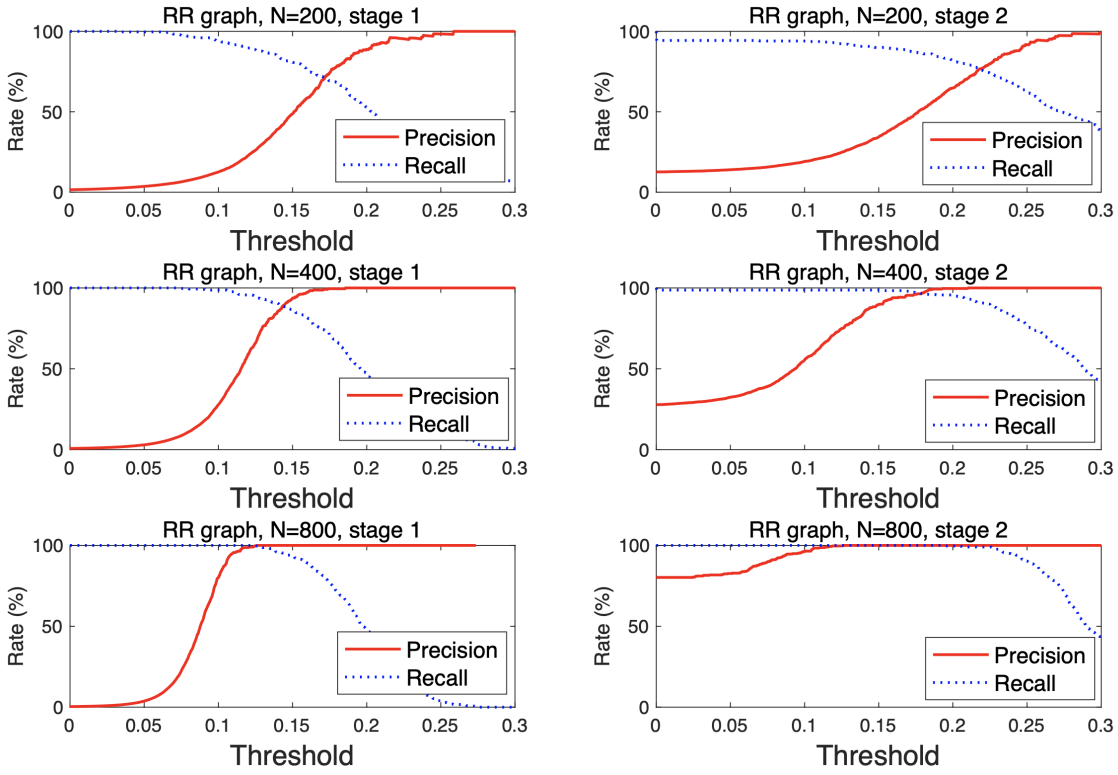


Figure 6: Precision and Recall for the RR graph using the two-stage estimator for different N in the case of $K = 0.4, \lambda = 0.1$, and $\alpha = 0.8$. The dotted and solid lines represent Recall and Precision, respectively. The left panels are for the first stage and are plotted against K_1, while the right ones are for the second stage and are plotted against K_2 after the first stage pruning with $K_1 = 0.1$. The results are obtained from 100 random runs.

work.

Another important direction we think is the use of the ℓ_1 regularization. This regularization is more popular in sparse estimation and also has been studied in inverse Ising problems [2, 14, 21, 22, 23]. Unfortunately, this regularization breaks the rotational symmetry of the coupling vector and hence the present analysis cannot be directly applied. It is necessary to invent additional theoretical techniques to overcome this, and such theoretical efforts are currently undergoing.

Acknowledgement

This work was supported by JSPS KAKENHI Nos. 17H00764, 18K11463, and 19H01812, and JST CREST Grant Number JPMJCR1912, Japan.

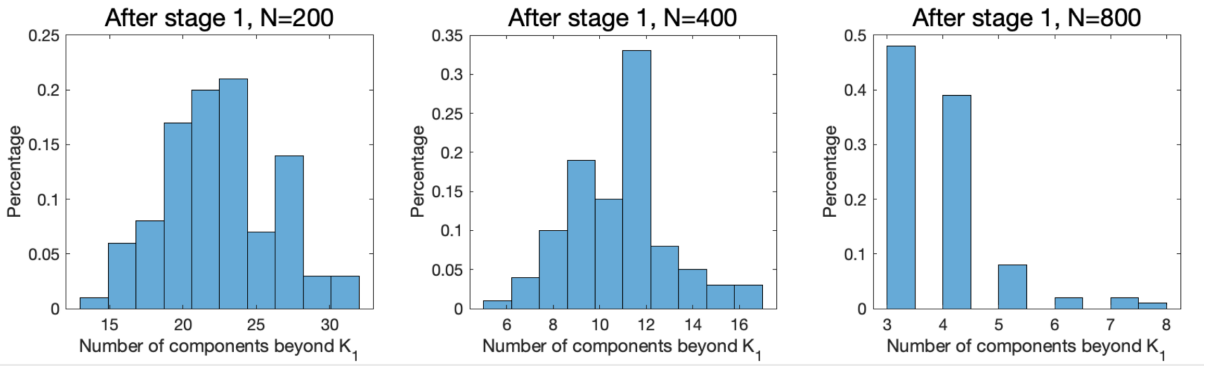


Figure 7: Histogram of the number of components selected after the first stage in the two-stage linear estimator for RR graph of different N in the case of $K = 0.4, \lambda = 0.1$, and $\alpha = 0.8$. For a fixed threshold $K_1 = 0.1$, as N increases, the number of components beyond the threshold K_1 decreases as the noise variance scales as $\mathcal{O}(1/N)$. The results are obtained from 100 random runs.

Appendices

Appendix A Computation of e^{NS}

According to the definition in (30), we have

$$e^{NS} = e^{-\lambda\beta Nn\sum_{j\in\Psi_d}\bar{J}_j^2}\int\prod_{a=1}^{n}d\boldsymbol{\Delta}^a e^{-\lambda\beta\sum_{a=1}^{n}\|\boldsymbol{\Delta}^a\|^2}\prod_{a=1}^{n}\delta\left(\sum_{i,j}\Delta_i^a C_{ij}^{\backslash 0}\Delta_j^a - NQ\right)$$
$$\times\prod_{a<b}\delta\left(\sum_{i,j}\Delta_i^a C_{ij}^{\backslash 0}\Delta_j^b - Nq\right). \tag{51}$$

The non-diagonality of $\boldsymbol{C}^{\backslash 0} = \left\{C_{ij}^{\backslash 0}\right\}$ will complicate subsequent computations; hence, we first diagonalize it by introducing an orthogonal matrix U such that $\boldsymbol{C}^{\backslash 0} = U^T\Lambda U$, where $\Lambda = \mathrm{diag}\left[\gamma_1, \ldots, \gamma_{\mathrm{N}-1}\right]$. Consequently, the term $\sum_{i,j}\Delta_i^a C_{ij}^{\backslash 0}\Delta_j^a$ becomes

$$\begin{aligned}\sum_{i,j}\Delta_i^a C_{ij}^{\backslash 0}\Delta_j^a &= (\triangle^a)^T\boldsymbol{C}^{\backslash 0}\triangle^a \\ &= (\triangle^a)^T U^T\Lambda U\triangle^a \\ &= (U\triangle^a)^T\Lambda\left(U\triangle^a\right) \\ &= \left(\tilde{\triangle}^a\right)^T\Lambda\tilde{\triangle}^a,\end{aligned} \tag{52}$$

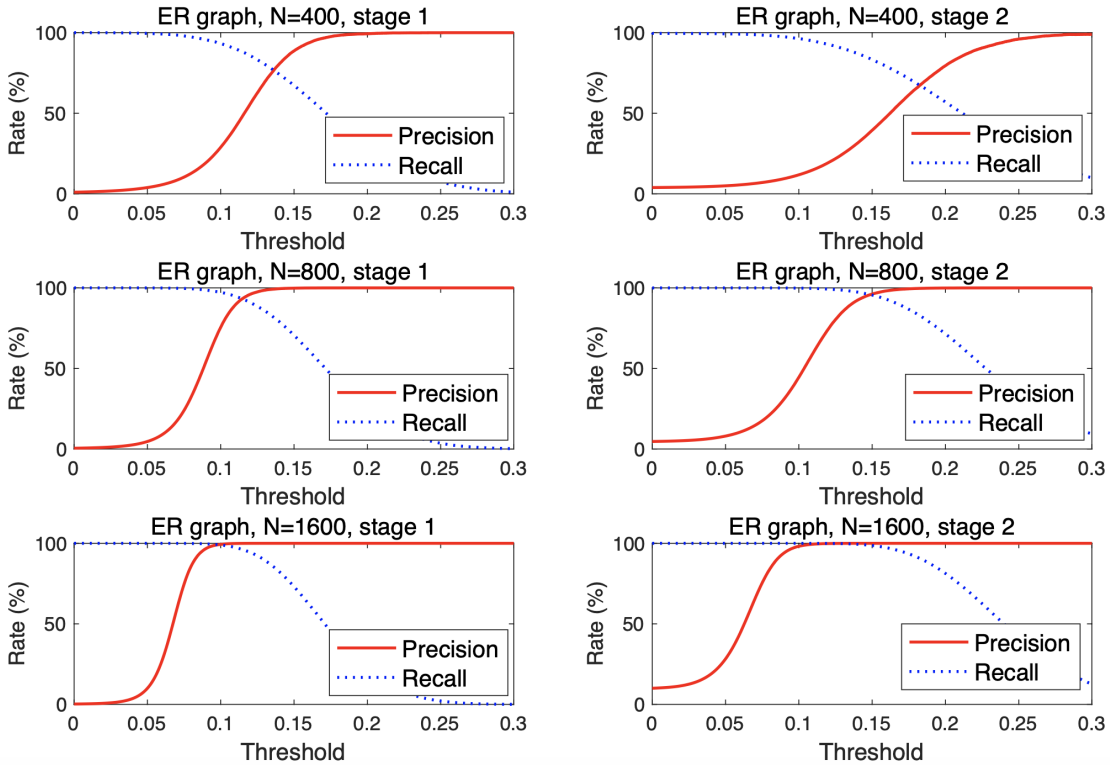


Figure 8: Precision and Recall for the ER graph using the two-stage estimator for different N in the case of $K = 0.4$, $\lambda = 0.1$, $\bar{c} = 4$, and $\alpha = 0.9$. The dotted and solid lines represent Recall and Precision, respectively. The left panels are for the first stage and are plotted against K_1, while the right ones are for the second stage and are plotted against K_2 after the first stage pruning with $K_1 = 0.05$. Owing to the finite size effect, exact perfect recovery is not achieved (though when $N = 1600$ 99.90% empirical Recall and 99.90% empirical Precision can be achieved simultaneously), but the improving tendency as N increases is observed, implying perfect recovery in the limit $N \to \infty$. Ten different ER graphs are generated, each with two independent MC samplings, and learning is then conducted for all $i = 0, ..., N-1$.

where $\tilde{\triangle}^a = U\triangle^a$. Similarly, $\sum_{i,j} \Delta_i^a C_{ij}^{\setminus 0} \Delta_j^b = \left(\tilde{\triangle}^a\right)^T \Lambda \tilde{\triangle}^b$, and $\left\|\tilde{\triangle}^a\right\|^2 = \|\triangle^a\|^2$. By performing the variable transformation in (51) and denoting $\tilde{\triangle}$ as $\triangle$, we obtain

$$e^{NS} \doteq e^{-\lambda\beta N n \sum_{j\in\Psi_d} \bar{J}_j^2} \int \prod_{a=1}^{n} d\boldsymbol{\Delta}^a e^{-\lambda\beta \sum_{a=1}^{n} \|\boldsymbol{\Delta}^a\|^2} \times \prod_{a=1}^{n} \delta\left((\boldsymbol{\Delta}^a)^T \Lambda \boldsymbol{\Delta}^a - NQ\right) \prod_{a<b} \delta\left((\boldsymbol{\Delta}^a)^T \Lambda \boldsymbol{\Delta}^b - Nq\right). \tag{53}$$

Then, the delta functions can be expressed as integrals over auxiliary parameters using the Fourier transform of the delta function, i.e.,

$$\begin{cases} \delta\left((\boldsymbol{\Delta}^a)^T \Lambda \boldsymbol{\Delta}^a - NQ\right) = \int d\hat{Q} e^{\hat{Q}\left((\boldsymbol{\Delta}^a)^T \Lambda \boldsymbol{\Delta}^a - NQ\right)}, \\ \delta\left((\boldsymbol{\Delta}^a)^T \Lambda \boldsymbol{\Delta}^b - Nq\right) = \int d\hat{q} e^{\hat{q}\left((\boldsymbol{\Delta}^a)^T \Lambda \boldsymbol{\Delta}^b - Nq\right)}, \end{cases} \tag{54}$$

where the integration over $\hat{Q}, \hat{q}$ is on the imaginary axis. Hence, (53) can be rewritten as

$$\begin{aligned}
e^{NS} &= \int d\hat{Q}d\hat{q}e^{-N\left(n\hat{Q}Q+\frac{n(n-1)}{2}\hat{q}q\right)}e^{-\lambda\beta Nn\sum_{j\in\Psi_d}\bar{J}_j^2}\int\prod_{a=1}^{n}d\boldsymbol{\Delta}^a e^{-\lambda\beta\sum_{a=1}^{n}\|\boldsymbol{\Delta}^a\|^2} \\
&\quad\times\exp\left\{\hat{Q}\sum_a(\boldsymbol{\Delta}^a)^T\Lambda\boldsymbol{\Delta}^a+\hat{q}\sum_{a<b}(\boldsymbol{\Delta}^a)^T\Lambda\boldsymbol{\Delta}^b\right\}, \\
&= \int d\hat{Q}d\hat{q}e^{-N\left(n\hat{Q}Q+\frac{n(n-1)}{2}\hat{q}q\right)}e^{-\lambda\beta N\sum_{j\in\Psi_d}\bar{J}_j^2}\int\prod_{a=1}^{n}d\boldsymbol{\Delta}^a e^{-\lambda\beta\sum_{a=1}^{n}\|\boldsymbol{\Delta}^a\|^2} \\
&\quad\times\exp\left\{\left(\hat{Q}-\frac{\hat{q}}{2}\right)\sum_a(\boldsymbol{\Delta}^a)^T\Lambda\boldsymbol{\Delta}^a+\frac{\hat{q}}{2}\sum_{a,b}(\boldsymbol{\Delta}^a)^T\Lambda\boldsymbol{\Delta}^b\right\}, \\
&= \int d\hat{Q}d\hat{q}e^{S_X}\int\prod_{a=1}^{n}d\boldsymbol{\Delta}^a e^{U},
\end{aligned} \tag{55}$$

where

$$S_X \doteq -N\left(\lambda\beta n\sum_{j\in\Psi_d}\bar{J}_j^2+n\hat{Q}Q+\frac{n(n-1)}{2}\hat{q}q\right), \tag{56}$$

$$\begin{aligned}
U \doteq& -\lambda\beta\sum_a\|\boldsymbol{\Delta}^a\|^2 \\
&+\left(\hat{Q}-\frac{\hat{q}}{2}\right)\sum_a(\boldsymbol{\Delta}^a)^T\Lambda\boldsymbol{\Delta}^a+\frac{\hat{q}}{2}\sum_{a,b}(\boldsymbol{\Delta}^a)^T\Lambda\boldsymbol{\Delta}^b.
\end{aligned} \tag{57}$$

Note that in (57), different replicas $\boldsymbol{\Delta}^a$, $\boldsymbol{\Delta}^b$ are coupled with each other, which makes it difficult to compute the integration. To overcome this problem, the Hubbard–Stratonovich transformation is used, i.e.,

$$e^{\frac{cy^2}{2}} = \frac{1}{\sqrt{2\pi c}}\int e^{-\frac{x^2}{2c}+xy}dx. \tag{58}$$

To apply it, we rewrite the term $\sum_{a,b}(\boldsymbol{\Delta}^a)^T\Lambda\boldsymbol{\Delta}^b$ as

$$\sum_{a,b}(\boldsymbol{\Delta}^a)^T\Lambda\boldsymbol{\Delta}^b = \sum_{a,b}\sum_i\gamma_i\triangle_i^a\triangle_i^b = \sum_i\gamma_i\left(\sum_a\triangle_i^a\right)^2 \tag{59}$$

so that

$$\begin{aligned}
e^{\frac{\hat{q}}{2}\sum_{a,b}(\triangle^a)^T\Lambda\triangle^b} &= \prod_i e^{\frac{\gamma_i\hat{q}(\sum_a\triangle_i^a)^2}{2}} \\
&= \prod_i\int\frac{dz_i}{\sqrt{2\pi}}e^{-\frac{z_i^2}{2}+\sqrt{\gamma_i\hat{q}}z_i\left(\sum_a\triangle_i^a\right)} \\
&= \prod_i\int\mathcal{D}z_i e^{\sqrt{\gamma_i\hat{q}}z_i\left(\sum_a\triangle_i^a\right)},
\end{aligned} \tag{60}$$

where the change of variable $x_i = \sqrt{\gamma_i \hat{q}} z_i$ is applied and $\mathcal{D}z_i = \frac{dz_i}{\sqrt{2\pi}} e^{-\frac{z_i^2}{2}}$. Consequently, different replicas are decoupled and we have

$$\begin{aligned}
\int \prod_{a=1}^{n} d\mathbf{\Delta}^a e^U =& \int \prod_{a=1}^{n} d\mathbf{\Delta}^a \exp\{-\lambda\beta \sum_a \|\triangle^a\|^2 \\
&+ \left(\hat{Q} - \frac{\hat{q}}{2}\right) \sum_a (\triangle^a)^T \Lambda \triangle^a\} \prod_i \int \mathcal{D}z_i e^{\sqrt{\gamma_i \hat{q}} z_i (\sum_a \triangle_i^a)} \\
=& \int \prod_i \mathcal{D}z_i \int \prod_{a=1}^{n} d\triangle^a \prod_a \exp\{-\lambda\beta \sum_i (\triangle_i^a)^2 \\
&+ \left(\hat{Q} - \frac{\hat{q}}{2}\right) \sum_i \gamma_i (\triangle_i^a)^2 + \sum_i \sqrt{\gamma_i \hat{q}} z_i \triangle_i^a\} \\
=& \int \prod_i \mathcal{D}z_i \int \prod_{a=1}^{n} d\triangle^a \prod_a \exp\{\sum_i \left[\left(\hat{Q} - \frac{\hat{q}}{2}\right) \gamma_i - \lambda\beta\right] (\triangle_i^a)^2 \\
&+ \sum_i \left(\sqrt{\gamma_i \hat{q}} z_i\right) \triangle_i^a\}. \qquad (61)
\end{aligned}$$

Since

$$\int dx e^{-Ax^2 + Bx} = \sqrt{\frac{\pi}{A}} e^{\frac{B^2}{4A}}, \qquad (62)$$

then

$$\begin{aligned}
&\int d\triangle_i^a \exp\left\{\left[\left(\hat{Q} - \frac{\hat{q}}{2}\right) \gamma_i - \lambda\beta\right] (\triangle_i^a)^2 + \left(\sqrt{\gamma_i \hat{q}} z_i\right) \triangle_i^a\right\} \\
=& \sqrt{\frac{2\pi}{\gamma_i \left(\hat{q} - 2\hat{Q} + 2\lambda\beta/\gamma_i\right)}} \exp\left[\frac{1}{2} \frac{\left(\sqrt{\hat{q}} z_i\right)^2}{\hat{q} - 2\hat{Q} + 2\lambda\beta/\gamma_i}\right]. \qquad (63)
\end{aligned}$$

Substituting (63) into (61), we have

$$\begin{aligned}
\int \prod_{a=1}^{n} d\triangle^a e^U =& \int \prod_i \mathcal{D}z_i \times \\
&\exp\left\{n \left[\sum_i \frac{1}{2} \frac{\left(\sqrt{\hat{q}} z_i\right)^2}{\hat{q} - 2\hat{Q} + 2\lambda\beta/\gamma_i} + \frac{1}{2} \log 2\pi - \frac{1}{2} \log \gamma_i - \frac{1}{2} \log\left(\hat{q} - 2\hat{Q} + 2\lambda\beta/\gamma_i\right)\right]\right\}. \qquad (64)
\end{aligned}$$

Consequently, the original high-dimensional integration reduces to a product of one-dimensional integrations w.r.t. z_i, independently.

$$\int \mathcal{D}z_i \exp\left[\frac{1}{2} \frac{n\left(\sqrt{\hat{q}} z_i\right)^2}{\hat{q} - 2\hat{Q} + 2\lambda\beta/\gamma_i}\right] = \sqrt{\frac{1}{1 - \frac{n\hat{q}}{\hat{q} - 2\hat{Q} + 2\lambda\beta/\gamma_i}}}. \qquad (65)$$

Then, we obtain

$$\int \prod_{a=1}^{n} d\triangle^a e^U = \exp\{-\frac{1}{2}\sum_i \log\left(1 - \frac{n\hat{q}}{\hat{q} - 2\hat{Q} + 2\lambda\beta/\gamma_i}\right) + \frac{N}{2}\log 2\pi - \frac{1}{2}\sum_i \log\gamma_i - \frac{1}{2}\sum_i \log\left(\hat{q} - 2\hat{Q} + 2\lambda\beta/\gamma_i\right)\}. \tag{66}$$

Thus,

$$\begin{aligned}\lim_{n\to 0}\frac{S}{n} &= \underset{\hat{q},\hat{Q}}{\text{Extr}}\left\{\lim_{n\to 0}\frac{\log\int d\hat{Q}d\hat{q}e^{S_X}\int\prod_{a=1}^{n}d\triangle^a e^U}{Nn}\right\} \\ &= \underset{\hat{q},\hat{Q}}{\text{Extr}}\{-\left(\lambda\beta\sum_{j\in\Psi_d}\bar{J}_j^2 + \hat{Q}Q - \frac{1}{2}\hat{q}q\right) + \frac{\hat{q}}{2N}\sum_i \frac{1}{\hat{q} - 2\hat{Q} + 2\lambda\beta/\gamma_i} \\ &+ \frac{1}{2}\log 2\pi - \frac{1}{2N}\sum_i \log\gamma_i - \frac{1}{2N}\sum_i \log\left(\hat{q} - 2\hat{Q} + 2\lambda\beta/\gamma_i\right)\},\end{aligned} \tag{67}$$

where $\underset{\hat{q},\hat{Q}}{\text{Extr}}\{\cdot\}$ denotes the extreme operation over $\hat{q}, \hat{Q}$. The summation in (67) is difficult to calculate. However, in the large system limit, the summation converges to the integration, which leads to

$$\begin{aligned}\lim_{n\to 0}\frac{S}{n} =& \underset{\hat{q},\hat{Q}}{\text{Extr}}\{-\left(\lambda\beta\sum_{j\in\Psi_d}\bar{J}_j^2 + \hat{Q}Q - \frac{1}{2}\hat{q}q\right) + \frac{\hat{q}}{2\beta}G_1\left(\frac{\hat{q} - 2\hat{Q}}{\beta}\right) \\ &+ \frac{1}{2}\log 2\pi - \frac{1}{2N}\text{Tr}\log\left(\boldsymbol{C}^{\setminus 0}\right)^{-1} - \frac{1}{2}G_2\left(\frac{\hat{q} - 2\hat{Q}}{\beta}\right) - \frac{1}{2}\log\beta\},\end{aligned} \tag{68}$$

where

$$G_1(x) = \int \frac{d\eta\rho(\eta)}{x + 2\lambda\eta}, \tag{69}$$

$$G_2(x) = \int d\eta\rho(\eta)\log(x + 2\lambda\eta). \tag{70}$$

Consequently, in (68), the extremization w.r.t. $\hat{q}$, $\hat{Q}$ leads to

$$\begin{cases} q = -\frac{\hat{q}}{\beta^2}G_1'\left(\frac{\hat{q} - 2\hat{Q}}{\beta}\right), \\ Q - q = \frac{1}{\beta}G_1\left(\frac{\hat{q} - 2\hat{Q}}{\beta}\right). \end{cases} \tag{71}$$

Therefore, we obtain

$$\begin{aligned}\lim_{n\to 0}\frac{S}{n} =& -\lambda\beta\sum_{j\in\Psi_d}\bar{J}_j^2 + \frac{Q\beta}{2}G_1^{-1}(\beta(Q - q)) - \frac{1}{2}G_2\left(G_1^{-1}(\beta(Q - q))\right) \\ &+ \frac{1}{2}\log\frac{2\pi}{\beta} - \frac{1}{2N}\text{Tr}\log\left(\boldsymbol{C}^{\setminus 0}\right)^{-1}.\end{aligned} \tag{72}$$

Appendix B Computation of L

The definition of L is given in (31), which is

$$L \doteq \sum_{s_0, \boldsymbol{s}_{\Psi_d}} P\left(s_0, \boldsymbol{s}_{\Psi_d} | J^*\right) \int \prod_{a=1}^{n} dh_{\triangle}^{a} P_{\text{cav}}\left(\left\{h_{\triangle}^{a}\right\}_a | \left\{\boldsymbol{\Delta}^a\right\}_a\right) e^{-\beta \sum_{a=1}^{n} \Phi\left(s_0\left(\sum_{j\in\Psi_d} \bar{J}_j s_j + h_{\triangle}^{a}\right)\right)}. \quad (73)$$

Using the cavity method, the local fields $h_{\triangle}^{a}, a = 1, \ldots, n$ follow a joint Gaussian distribution with zero mean (paramagnetic assumption) and covariances as

$$\left\langle h_a h_b \right\rangle^{\backslash 0} = Q\delta_{ab} + (1 - \delta_{ab})\, q. \quad (74)$$

Then, we can introduce two auxiliary i.i.d. Gaussian random variables v_a, z with zero mean and unit variance, by which the local fields can be written in a compact form

$$h_a = \sqrt{Q - q} v_a + \sqrt{q} z \quad (75)$$

so that L in (73) can be equivalently written as

$$\begin{aligned}
L &\doteq \sum_{s_0, \boldsymbol{s}_{\Psi_d}} P\left(s_0, \boldsymbol{s}_{\Psi_d} | J^*\right) \int \prod_{a=1}^{n} dh_{\triangle}^{a} P_{\text{cav}}\left(\left\{h_{\triangle}^{a}\right\}_a | \left\{\boldsymbol{\Delta}^a\right\}_a\right) e^{-\beta \sum_{a=1}^{n} \Phi\left(s_0\left(\sum_{j\in\Psi_d} \bar{J}_j s_j + h_{\triangle}^{a}\right)\right)} \\
&= \sum_{s_0, \boldsymbol{s}_{\Psi_d}} P\left(s_0, \boldsymbol{s}_{\Psi_d} | J^*\right) \int \mathcal{D}z \prod_{a} \mathcal{D}v_a e^{-\beta \sum_{a=1}^{n} \Phi\left(s_0\left(\sum_{j\in\Psi_d} \bar{J}_j s_j + \sqrt{Q-q} v_a + \sqrt{q} z\right)\right)} \\
&= \sum_{s_0, \boldsymbol{s}_{\Psi_d}} P\left(s_0, \boldsymbol{s}_{\Psi_d} | J^*\right) \int \mathcal{D}z \left[\underbrace{\int \mathcal{D}v e^{-\beta \Phi\left(s_0\left(\sum_{j\in\Psi_d} \bar{J}_j s_j + \sqrt{Q-q} v + \sqrt{q} z\right)\right)}}_{A}\right]^n \\
&= \sum_{s_0, \boldsymbol{s}_{\Psi_d}} P\left(s_0, \boldsymbol{s}_{\Psi_d} | J^*\right) E_z\left(A^n\right), \quad (76)
\end{aligned}$$

where $E_z\left(A^n\right) = \int \mathcal{D}z A^n$. Then, using the replica formula, we have

$$\begin{aligned}
\lim_{n\to 0} \frac{1}{n} \log L &= \lim_{n\to 0} \frac{\log \sum_{s_0, \boldsymbol{s}_{\Psi_d}} P\left(s_0, \boldsymbol{s}_{\Psi_d} | J^*\right) E_z\left(A^n\right)}{n} \\
&= E_z\left[\sum_{s_0, \boldsymbol{s}_{\Psi_d}} P\left(s_0, \boldsymbol{s}_{\Psi_d} | J^*\right) A\right] \\
&= \sum_{s_0, \boldsymbol{s}_{\Psi_d}} P\left(s_0, \boldsymbol{s}_{\Psi_d} | J^*\right) \int \mathcal{D}z \log \int \mathcal{D}v e^{-\beta \Phi\left(s_0\left(\sum_{j\in\Psi_d} \bar{J}_j s_j + \sqrt{Q-q} v + \sqrt{q} z\right)\right)}. \quad (77)
\end{aligned}$$

To further simplify the result, let $y = s_0\left(\sum_{j\in\Psi_d}\bar{J}_j s_j + \sqrt{Q-q}v + \sqrt{q}z\right)$. Consequently, we obtain

$$\begin{aligned}
&\int \mathcal{D}v e^{-\beta\Phi\left(s_0\left(\sum_{j\in\Omega}\bar{J}_j s_j+\sqrt{Q-q}v+\sqrt{q}z\right)\right)} \\
=&\int \frac{dv}{\sqrt{2\pi}} e^{-\frac{v^2}{2}} e^{-\beta\Phi(y)} \\
=&\int \frac{dy}{\sqrt{2\pi\left(Q-q\right)}} e^{-\frac{\left[y-s_0\left(\sum_{j\in\Omega}\bar{J}_j s_j+\sqrt{q}z\right)\right]^2}{2(Q-q)}} e^{-\beta\Phi(y)},
\end{aligned} \tag{78}$$

so that

$$\begin{aligned}
\lim_{n\to 0}\frac{1}{n}\log L &= \sum_{s_0,\boldsymbol{s}_{\Psi_d}} P\left(s_0,\boldsymbol{s}_{\Psi_d}|J^*\right)\int \mathcal{D}z \log \int \frac{dy}{\sqrt{2\pi\left(Q-q\right)}} e^{-\frac{\left[y-s_0\left(\sum_{j\in\Psi_d}\bar{J}_j s_j+\sqrt{q}z\right)\right]^2}{2(Q-q)}} e^{-\beta\Phi(y)} \\
&= \sum_{s_0,\boldsymbol{s}_{\Psi_d}} P\left(s_0,\boldsymbol{s}_{\Psi_d}|J^*\right)\int \mathcal{D}z \max_y \left[-\frac{\left(y-s_0\left(\sqrt{q}z+\sum_{j\in\Psi_d}\bar{J}_j s_j\right)\right)^2}{2\left(Q-q\right)} - \beta\Phi\left(y\right)\right].
\end{aligned} \tag{79}$$

Appendix C Derivation of Macroscopic Parameters

We use the technique of auxiliary variables in [5] by introducing the term $h_R\sum_{a=1}^{n}\|\boldsymbol{W}^a\|^2$ into $[Z^n]_{\mathcal{D}^M}$. Then, following the same procedure as that in Appendix A, we obtain

$$\begin{aligned}
\lim_{n\to 0}\frac{S}{n} = \operatorname*{Extr}_{\hat{q},\hat{Q}}\{&-\lambda\beta\sum_{j\in\Psi_d}\bar{J}_j^2 - \hat{Q}Q + \frac{1}{2}\hat{q}q + \frac{1}{2}\frac{1}{N}\sum_i \frac{\gamma_i\hat{q}}{\left(\hat{q}-2\hat{Q}\right)\gamma_i + 2\left(\lambda\beta - h_R\right)} \\
&- \frac{1}{2N}\sum_i \log\left(\hat{q}-2\hat{Q}+2\left(\lambda\beta-h_R\right)/\gamma_i\right) - \frac{1}{2N}\sum_i\log\gamma_i\}.
\end{aligned} \tag{80}$$

Thus, the macroscopic parameter $R = \frac{1}{N}\sum_{j\in\bar{\Psi}_d}\triangle_j^2$ can be derived using the derivative of the free energy, i.e.,

$$\begin{aligned}
R &= \lim_{h_R\to 0}\frac{\partial}{\partial h_R}\lim_{n\to 0}\frac{S}{n} \\
&= \frac{1}{N}\sum_i \frac{\hat{q}/\gamma_i}{\left(\hat{q}-2\hat{Q}+2\lambda\beta/\gamma_i\right)^2} + \frac{1}{N}\sum\frac{1/\gamma_i}{\hat{q}-2\hat{Q}+2\lambda\beta/\gamma_i} \\
&= \frac{\hat{q}}{\beta^2}\frac{1}{N}\sum_i \frac{1/\gamma_i}{\left(\frac{\hat{q}-2\hat{Q}}{\beta}+2\lambda/\gamma_i\right)^2} + \frac{1}{\beta}\frac{1}{N}\sum\frac{1/\gamma_i}{\frac{\hat{q}-2\hat{Q}}{\beta}+2\lambda/\gamma_i} \\
&= \frac{\hat{q}}{\beta^2}\frac{1}{N}\sum_i \frac{1/\gamma_i}{\left(\frac{\hat{q}-2\hat{Q}}{\beta}+2\lambda/\gamma_i\right)^2} + \underbrace{\frac{1}{\beta}\frac{1}{N}\sum\frac{1/\gamma_i}{a+2\lambda/\gamma_i}}_{\to 0\ (\beta\to\infty)} \\
&= q\frac{G_3'\left(\kappa\right)}{G_1'\left(\kappa\right)},
\end{aligned} \tag{81}$$

where

$$G_3(x) = \int \frac{d\eta \rho(\eta)\eta}{(x+2\lambda\eta)}. \tag{82}$$

Appendix D Numerical Solutions

In general, there is no analytic solution to the EOS equations in Section 3.3, but they can be easily solved using numerical methods.

First, we compute $\hat{y}$ by substituting $\Phi(y) = (y-1)^2$ into (40), which yields

$$\hat{y} = \frac{s_0\left(\sqrt{Q}z + \sum_{j\in\Psi_d}\bar{J}_j s_j\right) + 2G_1(\kappa)}{1+2G_1(\kappa)}, \tag{83}$$

from which we obtain

$$\begin{cases} \int \mathcal{D}z \frac{\partial\Phi(y)}{\partial y}\mid_{y=\hat{y}} = 2\frac{s_0\sum_{j\in\Psi_d}\bar{J}_j s_j - 1}{1+2G_1(\kappa)}, \\ \int \mathcal{D}z z \frac{\partial\Phi(y)}{\partial y}\mid_{y=\hat{y}} = \frac{2s_0\sqrt{Q}}{1+2G_1(\kappa)}, \\ \int \mathcal{D}z \left(\frac{\partial\Phi(y)}{\partial y}\mid_{y=\hat{y}}\right)^2 = 4\frac{Q+\left(\sum_{j\in\Psi_d}\bar{J}_j s_j\right)^2 - 2s_0\left(\sum_{j\in\Psi_d}\bar{J}_j s_j\right)+1}{[1+2G_1(\kappa)]^2}. \end{cases} \tag{84}$$

The mean estimates $\left(\bar{J}_j\right)_{j\in\Psi_d}$ can also be evaluated by the extremization condition, i.e.,

$$0 = 2\lambda\bar{J}_j + \alpha\sum_{s_0,\boldsymbol{s}_{\Psi_d}} P(s_0,\boldsymbol{s}_{\Psi_d}|J^*)\int \mathcal{D}z\frac{\partial\Phi(y)}{\partial y}\mid_{y=\hat{y}} s_0 s_j,\ j\in\Psi_d. \tag{85}$$

Hence, the mean estimates $\left(\bar{J}_j\right)_{j\in\Psi_d}$ can be evaluated from (85) by solving the linear equations

$$(1+2\lambda/\kappa)\bar{J}_j + \sum_{i\in\Psi_d, i\neq j}\bar{J}_i\langle s_i s_j\rangle - \langle s_0 s_j\rangle = 0,\ j\in\Psi_d, \tag{86}$$

where $\langle s_i s_j\rangle$ denotes the average w.r.t. the joint distribution $P(s_0,\boldsymbol{s}_{\Psi_d}|J^*)$.

The macroscopic parameters κ and Q can be obtained by numerically solving the following equations

$$0 = \kappa - \frac{2\alpha}{1+2G_1(\kappa)}, \tag{87}$$

$$Q = \frac{4\alpha G_1'(\kappa)\left(2\left\langle s_0\sum_{j\in\Psi_d}\bar{J}_j s_j\right\rangle - \left\langle\left(\sum_{j\in\Psi_d}\bar{J}_j s_j\right)^2\right\rangle - 1\right)}{(1+2G_1(\kappa))^2 + 4\alpha G_1'(\kappa)}. \tag{88}$$

Appendix E Eigenvalue Distribution

From the replica analysis presented, the learning performance will depend on the eigenvalue distribution (EVD) $\rho(\eta)$ of the inverse correlation matrix $\left(\boldsymbol{C}^{\backslash 0}\right)^{-1}$. In general, it is difficult to obtain this EVD; however, for a particular teacher network, we can obtain the analytic solution of $\rho(\eta)$. In this section, we illustrate how to compute $\rho(\eta)$ of the random regular (RR) graph

as a representative example of sparse tree-like graphs. Assume that as $N \to \infty$, the EVD of $\left(\boldsymbol{C}^{\backslash 0}\right)^{-1}$ approaches that of $\boldsymbol{C}^{-1}$ in the large system limit, where $\boldsymbol{C}$ is the correlation matrix that corresponds to the teacher spin system. The Gibbs free energy is defined as

$$G\left(\boldsymbol{m}\right) = \max_{\boldsymbol{\theta}} \left\{ \boldsymbol{\theta}^T \boldsymbol{m} - \log Z\left(\boldsymbol{\theta}\right) \right\}, \tag{89}$$

where $Z\left(\boldsymbol{\theta}\right) = \sum_{\boldsymbol{s}} e^{\sum_{i<j} J_{ij} s_i s_j + \sum_i \theta_i s_i}$. It can be verified that the Hessian of $G\left(\boldsymbol{m}\right)$ is equal to the inverse correlation matrix, i.e., $\left[\boldsymbol{C}^{-1}\right]_{ij} = \frac{\partial G(\boldsymbol{m})}{\partial m_i \partial m_j}$. Consequently, we can focus on the computation of $G\left(\boldsymbol{m}\right)$ to obtain the EVD of $\boldsymbol{C}^{-1}$. The RR graph is characterized by a connectivity parameter c and constant coupling strength K. The inverse correlation matrix can be computed from the Hessian of the Gibbs free energy [6, 27, 28] as

$$\begin{aligned} \left[\boldsymbol{C}^{-1}\right]_{ij} &= \frac{\partial G\left(\boldsymbol{m}\right)}{\partial m_i \partial m_j} \\ &= \left(\frac{c}{1-\tanh^2 K} - c + 1 \right) \delta_{ij} - \frac{\tanh\left(J_{ij}\right)}{1-\tanh^2\left(J_{ij}\right)} \left(1-\delta_{ij}\right), \end{aligned} \tag{90}$$

and in matrix form, we have

$$\boldsymbol{C}^{-1} = \left(\frac{c}{1-\tanh^2 K} - c + 1 \right) \mathbf{I} - \frac{\tanh\left(\boldsymbol{J}\right)}{1-\tanh^2\left(\boldsymbol{J}\right)}. \tag{91}$$

Since the matrix $\frac{\tanh(\boldsymbol{J})}{1-\tanh^2(\boldsymbol{J})}$ is also a sparse coupling matrix with constant coupling strength $K_1 = \frac{\tanh(K)}{1-\tanh^2(K)}$ and fixed connectivity c, the corresponding eigenvalue (denoted as ξ) distribution can be calculated as [29]

$$\rho_\xi\left(\xi\right) = \frac{c\sqrt{4K_1^2\left(c-1\right) - \xi^2}}{2\pi\left(K_1^2 c^2 - \xi^2\right)}, \ |\xi| \le 2K_1\sqrt{c-1}. \tag{92}$$

From (91), the eigenvalue η of $\boldsymbol{C}^{-1}$ is

$$\eta_i = \frac{c}{1-\tanh^2 K} - c + 1 - \xi_i, \tag{93}$$

which, when combined with (92), readily yields the EVD of η as $N \to \infty$ as follows:

$$\begin{aligned} \rho\left(\eta\right) &= \rho_\xi \left(\frac{c}{1-\tanh^2 K} - c + 1 - \eta \right) \\ &= \frac{c\sqrt{4\left(\frac{\tanh(K)}{1-\tanh^2(K)}\right)^2\left(c-1\right) - \left(\frac{c}{1-\tanh^2 K} - c + 1 - \eta\right)^2}}{2\pi\left(\left(\frac{\tanh(K)}{1-\tanh^2(K)}\right)^2 c^2 - \left(\frac{c}{1-\tanh^2 K} - c + 1 - \eta\right)^2\right)}, \end{aligned} \tag{94}$$

where $\eta \in \left[\frac{c}{1-\tanh^2 K} - c + 1 - \frac{2\tanh(K)\sqrt{c-1}}{1-\tanh^2(K)}, \frac{c}{1-\tanh^2 K} - c + 1 + \frac{2\tanh(K)\sqrt{c-1}}{1-\tanh^2(K)} \right]$.

Appendix F Proof of Theorem 1

Although the proof in the previous study (the one in Sec. 3.3 in [6]) can be applied to the present case, we provide another proof by employing some specific properties of the linear regression, because some steps in this proof are essential for Theorem 2, which is beyond the applicable range of the proof in [6]. Note that the advantage of the proof in [6] is its generality: an arbitrary cost function and the nonzero external fields are treated.

Specifically, in this case, the linear equations in (46) reduce to

$$\sum_{i\in\Psi_d} \bar{J}_i \langle s_i s_j \rangle = \langle s_0 s_j \rangle \,,\ j \in \Psi_d. \tag{95}$$

In matrix form,

$$\boldsymbol{C}_d \bar{\boldsymbol{J}} = \boldsymbol{b}, \tag{96}$$

$$\bar{\boldsymbol{J}} = \begin{bmatrix} \bar{J}_1 \\ \bar{J}_2 \\ \vdots \\ \bar{J}_{|\Psi_d|} \end{bmatrix}, \boldsymbol{b} = \begin{bmatrix} \langle s_0 s_1 \rangle \\ \langle s_0 s_2 \rangle \\ \vdots \\ \langle s_0 s_{|\Psi_d|} \rangle \end{bmatrix}, \tag{97}$$

where $\boldsymbol{C}_d = \{\langle s_i s_j \rangle\}_{i,j\in\Psi_d}$ is the correlation matrix of spins $s_j, j \in \Psi_d$. Consequently, the estimates $\bar{\boldsymbol{J}} = \left(\bar{J}_j\right)_{j\in\Psi_d}$ can be computed as $\bar{\boldsymbol{J}} = \boldsymbol{C}_d^{-1}\boldsymbol{b}$.

On the one hand, the full correlation matrix $\boldsymbol{C}_{0d} = \{\langle s_i s_j \rangle\}_{i,j\in\{0,\Psi_d\}}$ of spins $s_j,\ j \in \{0, \Psi_d\}$ can be represented as

$$\boldsymbol{C}_{0d} = \begin{bmatrix} 1 & \boldsymbol{b}^T \\ \boldsymbol{b} & \boldsymbol{C}_d \end{bmatrix}. \tag{98}$$

Thus, according to the block matrix inversion lemma, the inverse correlation matrix can be computed as

$$\boldsymbol{C}_{0d}^{-1} = \begin{bmatrix} F_{11}^{-1} & -F_{11}^{-1}\bar{\boldsymbol{J}}^T \\ -\bar{\boldsymbol{J}}F_{11}^{-1} & F_{22}^{-1} \end{bmatrix}, \tag{99}$$

where $F_{11} = 1 - \boldsymbol{b}^T\bar{\boldsymbol{J}}, F_{22} = \boldsymbol{C}_d - \boldsymbol{b}\boldsymbol{b}^T$.

On the other hand, for a sparse tree graph where s_i has connectivity c_i with true coupling J_{ij} with spin s_j, the inverse correlation matrix can be computed from the Hessian of the Gibbs free energy as [6, 27, 28]

$$\left[\boldsymbol{C}_{0d}^{-1}\right]_{ij} = \left(\sum_{k\in\partial i} \frac{1}{1-\tanh^2 J_{ik}} - c_i + 1\right)\delta_{ij} - \frac{\tanh\left(J_{ij}\right)}{1-\tanh^2 J_{ij}}\left(1-\delta_{ij}\right). \tag{100}$$

The two representations of $\boldsymbol{C}_{0d}^{-1}$ in (99) and (100) are equivalent; hence, the corresponding elements should be equal to each other. Specifically, we are interested in the first row, which corresponds to spin s_0. Denote $J_{0j} = J_j^*$ as the true couplings associated with spin s_0 in the

teacher network. Then, by the definition of Ω_1, we have $J_j^* = 0, j \notin \Omega_1$. Assuming that $c_0 = c = |\Omega_1|$, by comparing (99) and (100), it is easy to obtain

$$F_{11}^{-1} = \sum_{k\in\Omega_1} \frac{1}{1-\tanh^2 J_k^*} - c + 1, \tag{101}$$

$$\bar{J}_j F_{11}^{-1} = \frac{\tanh\left(J_j^*\right)}{1-\tanh\left(J_j^*\right)}, \tag{102}$$

which is the same as (47). The result of (48) can be readily obtained for constant couplings by substituting $J_j^* = K\text{sign}(J_j^*),\ j \in \Omega_1$, which completes the proof.

Appendix G Proof of Theorem 2

In this case, the estimate of $\bar{\boldsymbol{J}} = \left(\bar{J}_j\right)_{\ j\in\Psi_d}$ is the solution to the following linear equations:

$$\left(\boldsymbol{C}_d + \frac{2\lambda}{\kappa}\boldsymbol{I}\right)\bar{\boldsymbol{J}} = \boldsymbol{b}, \tag{103}$$

where $\boldsymbol{I}$ is the identity matrix. To evaluate the decay speed of $\left(\bar{J}_j\right)_{\ j\in\Psi_d}$ with the distance from s_0, we can compute the decay speed of $\left(\bar{J}_j\right)_{\ j\in\Psi_d}$ for two general NN spins s_i and s_j with distance 1. For notational simplicity, denote $\text{Dist}\,(s_i, s_j)$ as the distance between two spins s_i and s_j in the teacher Ising system. Then, for two NN spins s_i and s_j, $\text{Dist}\,(s_i, s_j) = 1$. Without loss of generality, using the gauge symmetry, we can assume that all the true couplings of the teacher Ising spin system are non-negative when the external field is absent and the paramagnet assumption holds; hence, each element in $\boldsymbol{C}_d$ and $\boldsymbol{b}$ is positive. Assuming that $\text{Dist}\,(s_i, s_0) = d-1$ and $\text{Dist}\,(s_j, s_0) = d$, then $\langle s_0 s_i\rangle = \theta^{d-1}$ and $\langle s_0 s_j\rangle = \theta^d$. In general, there are two cases.

Case 1: s_j is a leaf spin, which means that s_j is only directly connected to its parent spin s_i and has no children spins.

In this case, for any other spin $s_k, k \in \Psi_d, k \neq j$, we have $\text{Dist}\,(s_j, s_k) = \text{Dist}\,(s_i, s_k) + 1$. Then, the associated rows corresponding to s_i and s_j in (103) can be written as follows:

$$\begin{cases} \left(1+\frac{2\lambda}{\kappa}\right)\bar{J}_i + \theta\bar{J}_j + \sum_{k\in\Psi_d, k\neq i,j}\theta^{d_{ki}}\bar{J}_k = \theta^{d-1}, \\ \theta\bar{J}_i + \left(1+\frac{2\lambda}{\kappa}\right)\bar{J}_j + \sum_{k\in\Psi_d, k\neq i,j}\theta^{d_{ki}+1}\bar{J}_k = \theta^{d}, \end{cases}, \tag{104}$$

where $d_{ki} = \text{Dist}\,(s_i, s_k)$ and $d_{kj} = \text{Dist}\,(s_j, s_k)$. From (104), we can easily obtain

$$0 < \frac{\bar{J}_j}{\bar{J}_i} = \theta\frac{(D-1)}{D-\theta^2} < \theta, \tag{105}$$

where $D = 1 + \frac{2\lambda}{\kappa} > 1$, which implies that the ratio of the magnitude of $\bar{J}_j$ to that of its parent node $\bar{J}_i$ is smaller than θ whenever s_j is a leaf spin. Meanwhile, the signs of $\bar{J}_j$ and $\bar{J}_i$ are always the same, i.e., s_i has the same sign as its children spin s_j when s_j is a leaf spin.

Case 2: s_j is not a leaf spin but has its own direct children spins.

Denote Φ as the set of children spins of s_j. Then, for any spin $s_m, m \in \Phi$, we have $\text{Dist}(s_j, s_m) = \text{Dist}(s_i, s_m) - 1$. For any other spin $s_k, k \in \Psi_d/\Phi, k \neq j$, we have $\text{Dist}(s_j, s_k) = \text{Dist}(s_i, s_k) + 1$. Consequently, the associated rows corresponding to s_i and s_j in (103) can be written as follows:

$$\begin{cases} \left(1 + \frac{2\lambda}{\kappa}\right) \bar{J}_i + \theta \bar{J}_j + \sum_{k \in \Psi_d/\Phi, k \neq i,j} \theta^{d_{ki}} \bar{J}_k + \sum_{m \in \Phi} \theta^{d_{mj}+1} \bar{J}_m = \theta^{d-1}, \\ \theta \bar{J}_i + \left(1 + \frac{2\lambda}{\kappa}\right) \bar{J}_j + \sum_{k \in \Psi_d/\Phi, k \neq i,j} \theta^{d_{ki}+1} \bar{J}_k + \sum_{m \in \Phi} \theta^{d_{mj}} \bar{J}_m = \theta^{d}. \end{cases} \tag{106}$$

Then, denoting $D = 1 + \frac{2\lambda}{\kappa} > 1$, we obtain

$$\frac{\bar{J}_i}{\bar{J}_j} = \frac{D - \theta^2}{\theta (D-1)} + \frac{1}{\bar{J}_j} \sum_{m \in \Phi} \bar{J}_m \left(\theta^{d_{mj}} - \theta^{d_{mj}+2}\right). \tag{107}$$

Since Φ is the set of children spins of s_j, then for any $\bar{J}_m, m \in \Phi$, it can be deduced by induction that $\bar{J}_m$ has the same sign as $\bar{J}_j$ as follows.

First, if $s_m, m \in \Phi$ are all leaf spins, then using the result of case 1, $\bar{J}_m$ has the same sign as $\bar{J}_j$, i.e., $\bar{J}_m/\bar{J}_j > 0$. Second, if $s_m, m \in \Phi$ is not a leaf spin itself but has a leaf spin s_n, then $\bar{J}_n$ has the same sign as $\bar{J}_m$, and as with (107), we can obtain $\bar{J}_j/\bar{J}_m = \frac{D-\theta^2}{\theta(D-1)} + \frac{1}{\bar{J}_m} \bar{J}_n \left(\theta - \theta^2\right) > 0$; hence, $\bar{J}_m$ has the same sign as $\bar{J}_j$. By induction, the estimates of the children spins $\bar{J}_m, m \in \Phi$ will all have the same sign as $\bar{J}_j$.

Consequently, since (107), $\bar{J}_m/\bar{J}_j > 0, m \in \Phi$, and $0 < \theta < 1$, we have

$$\frac{\bar{J}_i}{\bar{J}_j} > \frac{D - \theta^2}{\theta (D-1)} > 0 \iff 0 < \frac{\bar{J}_j}{\bar{J}_i} < \frac{\theta (D-1)}{D - \theta^2}, \tag{108}$$

which implies that the ratio of the magnitude of $\bar{J}_j$ to that of its parent spin $\bar{J}_i$ is smaller than $\frac{\theta(D-1)}{D-\theta^2}$ for general s_j when it is not a leaf spin.

Summarizing both case 1 and case 2, for any two spins s_i and s_j with distance $\text{Dist}(s_i, s_j) = 1$, $\left|\frac{\bar{J}_j}{\bar{J}_i}\right| \leq \frac{\theta(D-1)}{D-\theta^2}$ always holds, which completes the proof.

References

[1] H Chau Nguyen, Riccardo Zecchina, and Johannes Berg. Inverse statistical problems: from the inverse ising problem to data science. *Advances in Physics*, 66(3):197–261, 2017.

[2] Erik Aurell and Magnus Ekeberg. Inverse ising inference using all the data. *Physical review letters*, 108(9):090201, 2012.

[3] Ludovica Bachschmid-Romano and Manfred Opper. Learning of couplings for random asymmetric kinetic ising models revisited: random correlation matrices and learning curves. *Journal of Statistical Mechanics: Theory and Experiment*, 2015(9):P09016, 2015.

[4] Johannes Berg. Statistical mechanics of the inverse ising problem and the optimal objective function. *Journal of Statistical Mechanics: Theory and Experiment*, 2017(8):083402, 2017.

[5] Ludovica Bachschmid-Romano and Manfred Opper. A statistical physics approach to learning curves for the inverse ising problem. *Journal of Statistical Mechanics: Theory and Experiment*, 2017(6):063406, 2017.

[6] Alia Abbara, Yoshiyuki Kabashima, Tomoyuki Obuchi, and Yingying Xu. Learning performance in inverse ising problems with sparse teacher couplings. *Journal of Statistical Mechanics: Theory and Experiment*, 2020(7):073402, 2020.

[7] David H Ackley, Geoffrey E Hinton, and Terrence J Sejnowski. A learning algorithm for boltzmann machines. *Cognitive science*, 9(1):147–169, 1985.

[8] Michael Habeck. Bayesian approach to inverse statistical mechanics. *Physical Review E*, 89(5):052113, 2014.

[9] Tamara Broderick, Miroslav Dudik, Gasper Tkacik, Robert E Schapire, and William Bialek. Faster solutions of the inverse pairwise ising problem. *arXiv preprint arXiv:0712.2437*, 2007.

[10] Hilbert J. Kappen and Francisco de Borja Rodríguez. Efficient learning in boltzmann machines using linear response theory. *Neural Computation*, 10(5):1137–1156, 1998.

[11] Toshiyuki Tanaka. Mean-field theory of boltzmann machine learning. *Physical Review E*, 58(2):2302, 1998.

[12] Vitor Sessak and Rémi Monasson. Small-correlation expansions for the inverse ising problem. *Journal of Physics A: Mathematical and Theoretical*, 42(5):055001, 2009.

[13] Julian Besag. Statistical analysis of non-lattice data. *Journal of the Royal Statistical Society: Series D (The Statistician)*, 24(3):179–195, 1975.

[14] Aurélien Decelle and Federico Ricci-Tersenghi. Pseudolikelihood decimation algorithm improving the inference of the interaction network in a general class of ising models. *Physical review letters*, 112(7):070603, 2014.

[15] Alexander Mozeika, Onur Dikmen, and Joonas Piili. Consistent inference of a general model using the pseudolikelihood method. *Physical Review E*, 90(1):010101, 2014.

[16] Marc Mezard and Andrea Montanari. *Information, physics, and computation*. Oxford University Press, 2009.

[17] Manfred Opper and David Saad. *Advanced mean field methods: Theory and practice*. MIT press, 2001.

[18] Hidetoshi Nishimori. *Statistical physics of spin glasses and information processing: an introduction*. Number 111. Clarendon Press, 2001.

[19] Mark Schmidt, Alexandru Niculescu-Mizil, Kevin Murphy, et al. Learning graphical model structure using ℓ_1-regularization paths. In *AAAI*, volume 7, pages 1278–1283, 2007.

[20] Martin J Wainwright and Michael Irwin Jordan. *Graphical models, exponential families, and variational inference*. Now Publishers Inc, 2008.

[21] Pradeep Ravikumar, Martin J Wainwright, John D Lafferty, et al. High-dimensional ising model selection using ℓ_1-regularized logistic regression. *The Annals of Statistics*, 38(3):1287–1319, 2010.

[22] Narayana P Santhanam and Martin J Wainwright. Information-theoretic limits of selecting binary graphical models in high dimensions. *IEEE Transactions on Information Theory*, 58(7):4117–4134, 2012.

[23] Guy Bresler. Efficiently learning ising models on arbitrary graphs. In *Proceedings of the forty-seventh annual ACM symposium on Theory of computing*, pages 771–782, 2015.

[24] Marc Vuffray, Sidhant Misra, Andrey Lokhov, and Michael Chertkov. Interaction screening: Efficient and sample-optimal learning of ising models. In *Advances in Neural Information Processing Systems*, pages 2595–2603, 2016.

[25] Andrey Y Lokhov, Marc Vuffray, Sidhant Misra, and Michael Chertkov. Optimal structure and parameter learning of ising models. *Science advances*, 4(3):e1700791, 2018.

[26] Aapo Hyvärinen. Consistency of pseudolikelihood estimation of fully visible boltzmann machines. *Neural Computation*, 18(10):2283–2292, 2006.

[27] Federico Ricci-Tersenghi. The bethe approximation for solving the inverse ising problem: a comparison with other inference methods. *Journal of Statistical Mechanics: Theory and Experiment*, 2012(08):P08015, 2012.

[28] H Chau Nguyen and Johannes Berg. Bethe–peierls approximation and the inverse ising problem. *Journal of Statistical Mechanics: Theory and Experiment*, 2012(03):P03004, 2012.

[29] Brendan D McKay. The expected eigenvalue distribution of a large regular graph. *Linear Algebra and its Applications*, 40:203–216, 1981.